

Intrinsic lifetime of Dirac plasmons in graphene

Alessandro Principi* and Giovanni Vignale

Department of Physics and Astronomy, University of Missouri, Columbia, Missouri 65211, USA

Matteo Carrega and Marco Polini

NEST, Istituto Nanoscienze-CNR and Scuola Normale Superiore, I-56126 Pisa, Italy

(Received 22 May 2013; revised manuscript received 18 October 2013; published 12 November 2013)

We calculate the *intrinsic* lifetime of a Dirac plasmon in a doped graphene sheet by analyzing the role of electron-electron interactions beyond the random phase approximation. The damping mechanism at work is intrinsic since it operates also in disorder-free samples and in the absence of lattice vibrations. We demonstrate that graphene's sublattice-pseudospin degree of freedom suppresses intrinsic plasmon losses with respect to those that occur in ordinary two-dimensional electron liquids. As a byproduct, we are able to present a microscopic calculation of the homogeneous dynamical conductivity at energies below the single-particle absorption threshold.

DOI: [10.1103/PhysRevB.88.195405](https://doi.org/10.1103/PhysRevB.88.195405)

PACS number(s): 73.20.Mf, 71.45.Gm, 78.67.Wj

I. INTRODUCTION

Plasmons are ubiquitous high-frequency collective density oscillations of an electron liquid, which occur both in metals and insulators.^{1,2} The study of optical phenomena in the nanoscale vicinity of metal surfaces, i.e., *nanoplasmonics*,^{3,4} revolves around the coupling between light and plasmons, which, in turn, enables the compression of electromagnetic energy to the nanometer scale of modern electronic devices. Of particular interest for novel applications is the study of the so-called “Dirac plasmons” (DPs)^{5–8} of the two-dimensional (2D) electron liquid in a doped graphene sheet,^{9–11} where the carriers are massless Dirac fermions (MDFs). The properties of DPs have been studied experimentally by a variety of spectroscopic methods¹² and their coupling to infrared light has been engineered in a number of ways.^{13–18} References 15 and 16, in particular, have revealed that the plasmon wavelength can be much smaller than the illumination wavelength and that DP properties are easily gate tunable, thus igniting the field of “graphene plasmonics.”¹²

Mathematically, a plasmon is an isolated pole of the density-density linear-response function $\chi_{nn}(q, \omega)$,^{1,2} that is found at a frequency $\Omega_p(q) = \omega_p(q) - i\Gamma_p(q)$, with $0 < \Gamma_p(q) \ll \omega_p(q)$, i.e., located slightly below the real axis. The real part of the DP dispersion relation $\omega_p(q)$ displays the usual dependence⁵ $\omega_p(q) \propto \sqrt{q}$ on wave vector q , typical of 2D electron gases (2DEGs).² The prefactor, however, displays certain peculiarities stemming from broken Galilean invariance.⁶ By using perturbation theory to first order in electron-electron (e-e) interactions,⁶ it was shown that the prefactor of the plasmon dispersion at long wavelengths is controlled by an interaction-enhanced Drude weight.^{6,7} This is a result that cannot be obtained on the basis of the random phase approximation (RPA).^{1,2} The long-wavelength DP dispersion has also been analyzed within the Landau theory of Fermi liquids.⁸

A key figure of merit of nanoplasmonics is the plasmon lifetime

$$\tau_p(q) = \frac{1}{2\Gamma_p(q)}, \quad (1)$$

or, equivalently, the inverse quality factor $\gamma_p(q) = [\tau_p(q)\omega_p(q)]^{-1}$. Plasmon damping is controlled by e-e,

electron-impurity, and electron-phonon scattering. Yan *et al.*¹⁹ have shown that the damping rate of mid-infrared DPs is strongly affected by substrate and intrinsic phonons. More recently, the role of electron-impurity scattering has been analyzed in Ref. 20. In this paper we present a theory of the *intrinsic* DP lifetime. By “intrinsic” we mean the contribution to τ_p that is solely determined by e-e collisions and therefore survives also in the complete absence of disorder and lattice vibrations.

For extreme concentration of electromagnetic energy the plasmon momenta q of interest are much larger than $q_{\text{light}} = \omega_{\text{ph}}/c$, where $\hbar\omega_{\text{ph}}$ is the free-space photon energy,^{14–16} but still much smaller than the Fermi wave number k_F for typical electron densities²¹ $n \sim 10^{11}–10^{12} \text{ cm}^{-2}$. For $q_{\text{light}} \ll q \ll k_F$ the DP dispersion satisfies the inequality $\hbar\omega_p(q) < 2\varepsilon_F$ and therefore a plasmon *cannot* decay by emitting single electron-hole pairs (Fig. 1)—a mechanism that would be captured by the RPA.⁵ Therefore, in this regime of momenta, the RPA erroneously predicts no damping whatsoever.^{2,22,23} To correct this, we carry out a calculation of τ_p for DPs in a doped graphene sheet by employing second-order perturbation theory in the strength of e-e interactions. Physically, the lifetime we calculate is determined by decay processes in which a plasmon emits *two* electron-hole pairs.^{2,22,23} Our final expression for τ_p is *exact* in the limit of a large number N_f of fermion flavors.²⁴ As a byproduct of our calculation, we are able to determine the dynamical conductivity of graphene for frequencies below the single-particle absorption threshold ($\hbar\omega < 2\varepsilon_F$). In this regime the dynamical conductivity is indeed controlled (at the leading nonvanishing order in the strength of e-e interactions) by the simultaneous excitation of two electron-hole pairs.

Our paper is organized as follows. In Sec. II we introduce the model Hamiltonian and all the basic definitions. In Sec. IV we describe the approach we have used to carry out the calculation of the intrinsic DP lifetime, which is based on a canonical transformation that exactly cancels, order-by-order in perturbation theory, the Coulomb interaction from the complete Hamiltonian. In Sec. V we explicitly derive the form of the generator of the canonical transformation up to first order in the Coulomb interaction. In Sec. VI we approximate this expression in the limit $q \rightarrow 0$ and $v_F q \ll \omega_p(q) \ll 2\varepsilon_F/\hbar$.

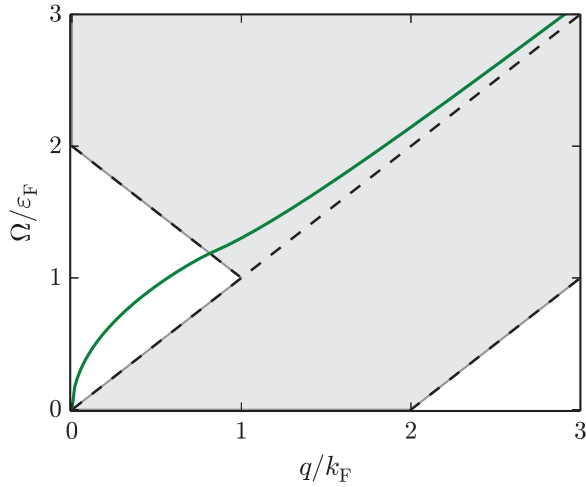


FIG. 1. (Color online) The RPA Dirac plasmon dispersion $\omega_p(q)$ (solid line) in units of the Fermi energy ε_F , plotted as a function of wave vector q in units of the Fermi wave vector k_F . In this plot we set the dimensionless parameter $\alpha_{ee} = 0.5$ [see Eq. (67) for the definition]. Within RPA the long-wavelength Dirac plasmon is a well-defined excitation since it lives outside the particle-hole continuum (shaded region). RPA thus (erroneously) predicts no damping of the collective mode at small q .

In Sec. VII we derive the expression for density-density linear response function, which is the fundamental input to calculate the Dirac plasmon lifetime, to second order in the strength of e-e interactions and in the so called “large- N ” limit. In this limit the second-order expression for the imaginary part of the density-density response function has the appealing form of a convolution of two single-particle spectra, which is also known in the electron-gas literature as “mode-decoupling formula.”² Our theoretical method allows us to unify the large- N expansion of diagrammatic perturbation theory with the mode-decoupling approximation,² providing a formal justification for the latter. Section VIII is devoted to the presentation of our main results. In Sec. IX we draw our main conclusions. Three Appendices report a number of useful intermediate algebraic steps and technical details.

II. MODEL AND BASIC DEFINITIONS

We describe π electrons in graphene by means of a one-orbital tight-binding (TB) model. To keep the model as simple as possible, we set to zero all the hopping parameters but the nearest-neighbor one. The low-energy MDF limit will be taken only at the very end of the calculation, *after* carrying out all the necessary algebraic manipulations. By following this procedure we avoid problems associated with the introduction of a rigid ultraviolet cutoff, which breaks gauge invariance⁶ and is responsible for the appearance of anomalous commutators.^{6,25}

The noninteracting Hamiltonian is (from now on we set $\hbar = 1$)

$$\hat{\mathcal{H}}_0 = \sum_{\mathbf{k} \in \text{BZ}, \alpha, \beta} \hat{\psi}_{\mathbf{k}, \alpha}^\dagger (\mathbf{f}_{\mathbf{k}} \cdot \boldsymbol{\sigma}_{\alpha\beta}) \hat{\psi}_{\mathbf{k}, \beta}, \quad (2)$$

where the operator $\hat{\psi}_{\mathbf{k}, \alpha}^\dagger$ ($\hat{\psi}_{\mathbf{k}, \alpha}$) creates (annihilates) an electron with Bloch momentum \mathbf{k} , which belongs to the sublattice¹⁰ $\alpha = A, B$. The vector $\mathbf{f}_{\mathbf{k}}$ is defined as¹⁰

$$\mathbf{f}_{\mathbf{k}} = -t \sum_{i=1}^3 (\text{Re}[e^{-i\mathbf{k} \cdot \boldsymbol{\delta}_i}], -\text{Im}[e^{-i\mathbf{k} \cdot \boldsymbol{\delta}_i}]). \quad (3)$$

Here $t \sim 2.8$ eV is the nearest-neighbor tunneling amplitude, while $\boldsymbol{\delta}_i$ ($i = 1, \dots, 3$) are the vectors which connect an atom to its three nearest neighbors, i.e., $\boldsymbol{\delta}_1 = a\sqrt{3}\hat{x}/2 + a\hat{y}/2$, $\boldsymbol{\delta}_2 = -a\sqrt{3}\hat{x}/2 + a\hat{y}/2$, and $\boldsymbol{\delta}_3 = -a\hat{y}$. Here $a \sim 1.42$ Å is the carbon-carbon distance in graphene. The sum over \mathbf{k} in Eq. (2) is restricted to the first Brillouin zone (BZ) and the Pauli matrices $\sigma_{\alpha\beta}^i$ ($i = x, y, z$) operate on the sublattice degrees of freedom.

The TB problem posed by the Hamiltonian (2) can be easily solved analytically.¹⁰ One finds the following eigenvalues $\varepsilon_{\mathbf{k}, \lambda} = \lambda|\mathbf{f}_{\mathbf{k}}|$, with $\lambda = \pm$. These two bands touch at two inequivalent points (K and K') in the hexagonal BZ. The low-energy MDF model is obtained from Eq. (2) by taking the limit $a \rightarrow 0$, while keeping the product ta constant. In this limit $\mathbf{f}_{\mathbf{K}+\mathbf{k}} \rightarrow v_F \mathbf{k}$, where $v_F = 3ta/2 \sim 10^6$ m/s is the density-independent Fermi velocity.

Introducing the field operator $\hat{c}_{\mathbf{k}, \lambda}^\dagger$ ($\hat{c}_{\mathbf{k}, \lambda}$) as the creation (annihilation) operator in the eigenstate representation, Eq. (2) can be rewritten as

$$\hat{\mathcal{H}}_0 = \sum_{\mathbf{k}, \lambda} \varepsilon_{\mathbf{k}, \lambda} \hat{c}_{\mathbf{k}, \lambda}^\dagger \hat{c}_{\mathbf{k}, \lambda}. \quad (4)$$

In the same representation the Hamiltonian describing e-e interactions reads²

$$\hat{\mathcal{H}}_{ee} = \frac{1}{2} \sum_{\mathbf{q}} v_{\mathbf{q}} \hat{n}_{\mathbf{q}} \hat{n}_{-\mathbf{q}}, \quad (5)$$

where the density operator is

$$\hat{n}_{\mathbf{q}} = \sum_{\mathbf{k}, \lambda, \lambda'} \mathcal{D}_{\lambda\lambda'}(\mathbf{k} - \mathbf{q}/2, \mathbf{k} + \mathbf{q}/2) \hat{c}_{\mathbf{k}-\mathbf{q}/2, \lambda}^\dagger \hat{c}_{\mathbf{k}+\mathbf{q}/2, \lambda'}, \quad (6)$$

and $v_{\mathbf{q}}$ is the 2D *discrete* Fourier transform of the real-space Coulomb interaction, which is a periodic function of the reciprocal-lattice vectors. Finally, in Eq. (6) we have introduced the “density vertex”

$$\mathcal{D}_{\lambda\lambda'}(\mathbf{k}, \mathbf{k}') = \frac{e^{i(\theta_{\mathbf{k}} - \theta_{\mathbf{k}'})/2} + \lambda\lambda' e^{-i(\theta_{\mathbf{k}} - \theta_{\mathbf{k}'})/2}}{2}, \quad (7)$$

with $\theta_{\mathbf{k}} = \text{Arg}[f_{\mathbf{k}, x} + if_{\mathbf{k}, y}]$. Here $\{f_{\mathbf{k}, i}, i = x, y\}$ denotes the Cartesian component of the vector $\mathbf{f}_{\mathbf{k}}$. In the low-energy MDF limit, $\theta_{\mathbf{K}+\mathbf{k}} \rightarrow \varphi_{\mathbf{k}}$, where $\varphi_{\mathbf{k}}$ is the angle between \mathbf{k} and the \hat{x} axis.

Note that in writing Eq. (5) we have neglected the one-body operator proportional to the total number of particles, which avoids self-interactions² since it has no effect on the calculations we will carry out below. The Dirac plasmon lifetime outside the particle-hole continuum is indeed determined by two-particle excitations only, which are generated by *two-body* operators.

For future purposes we also introduce the ‘‘pseudospin-density’’ vertices

$$S_{\lambda\lambda'}^{(x)}(\mathbf{k}, \mathbf{k}') = \frac{\lambda' e^{i(\theta_{\mathbf{k}} + \theta_{\mathbf{k}'})/2} + \lambda e^{-i(\theta_{\mathbf{k}} + \theta_{\mathbf{k}'})/2}}{2} \quad (8)$$

and

$$S_{\lambda\lambda'}^{(y)}(\mathbf{k}, \mathbf{k}') = \frac{\lambda' e^{i(\theta_{\mathbf{k}} + \theta_{\mathbf{k}'})/2} - \lambda e^{-i(\theta_{\mathbf{k}} + \theta_{\mathbf{k}'})/2}}{2i}. \quad (9)$$

In what follows we concentrate on a doped graphene sheet. For the sake of definiteness, we assume the system to be n doped. Results for a p -doped system can be easily obtained by appealing to the particle-hole symmetry of the model defined by Eqs. (2) and (5).

Our goal is to calculate the DP lifetime as defined in Eq. (1). To this end, we recall that the imaginary part $\Gamma_p(q)$ of the plasmon dispersion is controlled by the wave-vector- and frequency-dependent density-density linear response function² $\chi_{nn}(q, \omega)$:

$$\Gamma_p(q) = \frac{\text{Im}[\chi_{nn}(q, \omega)]}{\partial \text{Re}[\chi_{nn}(q, \omega)] / \partial \omega} \Big|_{\omega=\omega_p(q)}. \quad (10)$$

Since outside the single-particle electron-hole continuum $\text{Im}[\chi_{nn}(q, \omega)]$ starts at second order in e-e interactions, $\text{Re}[\chi_{nn}(q, \omega)]$ can be calculated to zeroth order and the real part of the plasmon frequency $\omega_p(q)$ can be evaluated within the well-known RPA:^{5,12}

$$\omega_p(q \ll k_F) = \sqrt{\frac{2D_0}{\epsilon}} q. \quad (11)$$

Here $D_0 = 4\varepsilon_F \sigma_{\text{uni}} / \hbar$ is the noninteracting Drude weight, $\varepsilon_F = \hbar v_F k_F$ is the Fermi energy, $\sigma_{\text{uni}} = N_f e^2 / (16\hbar)$ is the so-called universal optical conductivity,^{11,12} and $\epsilon = (\epsilon_1 + \epsilon_2) / 2$ is the average of the dielectric constants of the media above (ϵ_1) and below (ϵ_2) the graphene flake.^{10,11} Finally, $k_F = \sqrt{4\pi n / N_f}$ is the Fermi wave vector, with n the electron density.

In what follows we calculate $\text{Im}[\chi_{nn}(q, \omega)]$ to the lowest nonvanishing (i.e., the second) order in perturbation theory and in the limit $q \ll k_F$ and $v_F q \ll \omega \ll 2\varepsilon_F$.

III. THE CONTINUITY EQUATION IN THE TIGHT-BINDING MODEL

Within the TB model outlined above, the density-density and longitudinal current-current response functions satisfy the usual relation imposed by the continuity equation² [see Eq. (16) below]. To prove this statement, we first note that $[\hat{n}_q, \hat{n}_{q'}] = 0$ since the sum over momentum on the right-hand side of Eq. (6) is restricted to the first BZ. The density operator thus commutes with Eq. (5). We therefore find

$$i\partial_t \hat{n}_q = \sum_{\mathbf{k}, \lambda, \lambda'} \sum_j \hat{c}_{\mathbf{k}-q/2, \lambda}^\dagger \hat{c}_{\mathbf{k}+q/2, \lambda'} (\mathbf{f}_{\mathbf{k}+q/2} - \mathbf{f}_{\mathbf{k}-q/2})_j \times S_{\lambda\lambda'}^{(j)}(\mathbf{k} - \mathbf{q}/2, \mathbf{k} + \mathbf{q}/2) \equiv -\mathbf{q} \cdot \hat{\mathbf{j}}_q. \quad (12)$$

Here $\hat{\mathbf{j}}_q$ is the TB expression for the current operator.

We now remind the reader that a linear response function $\chi_{AB}(\omega)$, which describes the response of an operator \hat{B} to a potential which couples linearly to the operator \hat{A} , is related

to the so-called ‘‘Kubo product’’ by

$$\chi_{AB}(\omega) = \frac{1}{S} \langle \langle \hat{A}; \hat{B} \rangle \rangle_\omega, \quad (13)$$

where S is the 2D electron system area²⁶ and

$$\langle \langle \hat{A}; \hat{B} \rangle \rangle_\omega \equiv -i \int_0^\infty dt e^{i(\omega+i\eta)t} \langle [\hat{A}(t), \hat{B}] \rangle. \quad (14)$$

Note that the average $\langle \cdot \cdot \rangle$ in Eq. (14) is taken over the ground state of the interacting system. The Kubo product satisfies the following well-known² identities:

$$\begin{aligned} \langle \langle \hat{A}; \hat{B} \rangle \rangle_\omega &= \frac{1}{\omega} \langle [\hat{A}, \hat{B}] \rangle + \frac{1}{\omega} \langle \langle i\partial_t \hat{A}; \hat{B} \rangle \rangle_\omega \\ &= \frac{1}{\omega} \langle [\hat{A}, \hat{B}] \rangle - \frac{1}{\omega} \langle \langle \hat{A}; i\partial_t \hat{B} \rangle \rangle_\omega. \end{aligned} \quad (15)$$

Using the previous identities and the fact that the equal-time commutator of two Hermitian operators is anti-Hermitian, we finally get

$$\text{Im}[\chi_{nn}(q, \omega)] = \frac{q^2}{\omega^2} \text{Im}[\chi_{jj}^{(L)}(q, \omega)], \quad (16)$$

where $\chi_{jj}^{(L)}(q, \omega)$ is the longitudinal current-current response function. The longitudinal component of the current density operator $\hat{\mathbf{q}} \cdot \hat{\mathbf{j}}_q$ is defined by Eq. (12).

At first sight one might be confused by Eq. (16), since we are dealing with a TB model, which is not invariant under free-space translations. It is indeed well known (see also Appendix 7 in Ref. 2) that the response functions of the electron gas in a crystal are (i) matrices in the reciprocal-lattice vectors and (ii) depend on the wave vector \mathbf{q} (not only on its modulus $q \equiv |\mathbf{q}|$). The matrix structure of the linear response functions stems from the presence of an infinite number of bands. However, the one-orbital TB description of graphene adopted in this paper reduces the infinite band structure to the two π bands. For this reason, the response functions in Eq. (16) are scalars (rather than matrices) in the reciprocal-lattice vectors. Note that they contain all the information about both intra- and interband transitions. Moreover, in view of the low-energy MDF limit which will be taken at the very end of the calculation, and which restores rotational invariance, the response functions in Eq. (16) depend only on q .

IV. THE CANONICAL TRANSFORMATION

To proceed further in the evaluation of the density-density response function, we introduce a unitary transformation generated by a Hermitian operator \hat{F} :

$$\hat{\mathcal{H}}' = e^{i\hat{F}} (\hat{\mathcal{H}}_0 + \hat{\mathcal{H}}_{\text{ee}}) e^{-i\hat{F}}. \quad (17)$$

The operator \hat{F} is chosen in such a way as to cancel e-e interactions from the transformed Hamiltonian, i.e., to have $\hat{\mathcal{H}}' \equiv \hat{\mathcal{H}}_0$. This can be done systematically order-by-order in perturbation theory by expanding $\hat{F} = \hat{\mathbb{1}} + \hat{F}_1 + \hat{F}_2 + \dots$, where $\hat{\mathbb{1}}$ denotes the identity and \hat{F}_n denotes the n th order term in powers of a dimensionless parameter that controls the

strength of e-e interactions. We get

$$\begin{aligned} \hat{\mathcal{H}}' &= \hat{\mathcal{H}}_0 + \hat{\mathcal{H}}_{ee} + i[\hat{F}_1, \hat{\mathcal{H}}_0] \\ &+ i[\hat{F}_2, \hat{\mathcal{H}}_0] + i[\hat{F}_1, \hat{\mathcal{H}}_{ee}] - \frac{1}{2}[\hat{F}_1, [\hat{F}_1, \hat{\mathcal{H}}_0]] + \dots \end{aligned} \quad (18)$$

When we equate Eq. (18) to $\hat{\mathcal{H}}_0$ we obtain a chain of equations connecting $\hat{\mathcal{H}}_{ee}$ and $\hat{\mathcal{H}}_0$ to \hat{F}_n , which can be determined by solving the following infinite system of operator identities:

$$\begin{aligned} [\hat{\mathcal{H}}_0, i\hat{F}_1] &= \hat{\mathcal{H}}_{ee} \\ i[\hat{F}_2, \hat{\mathcal{H}}_0] + i[\hat{F}_1, \hat{\mathcal{H}}_{ee}] - \frac{1}{2}[\hat{F}_1, [\hat{F}_1, \hat{\mathcal{H}}_0]] &= 0 \\ &\dots \end{aligned} \quad (19)$$

For example, to eliminate e-e interactions up to first order, \hat{F}_1 must obey the first equality in Eq. (19), which can be easily solved (see Sec. V).

Note that after carrying out the transformation \hat{F} , both the ground state of $\hat{\mathcal{H}}'$ and the time evolution of the operators in the Heisenberg representation become noninteracting. This is clearly a significant simplification. The Kubo product in Eq. (14) is reduced to the evaluation of a noninteracting response function $\propto \langle \langle \hat{A}', \hat{B}' \rangle \rangle_{0, \omega}$. The subscript “0” here means that the average $\langle \dots \rangle$ is now performed over the ground state on the noninteracting system and that the time evolution is generated by $\hat{\mathcal{H}}_0$. However, the operators $\hat{A}' = e^{i\hat{F}} \hat{A} e^{-i\hat{F}}$ and $\hat{B}' = e^{i\hat{F}} \hat{B} e^{-i\hat{F}}$ become complicated since they are dressed by e-e interactions. For example, the imaginary part of the longitudinal current-current response function on the right-hand side of Eq. (16) obeys the following exact-eigenstate (Lehmann) representation:

$$\begin{aligned} \text{Im}[\chi_{jj}^{(L)}(q, \omega)] \\ = -\pi \sum_m \langle 0 | \hat{q} \cdot \hat{j}'_q | m \rangle \langle m | \hat{q} \cdot \hat{j}'_{-q} | 0 \rangle \delta(\omega - \omega_{m0}). \end{aligned} \quad (20)$$

Here $|0\rangle$ is the ground state of the noninteracting system, $|m\rangle$ is an excited state, and ω_{m0} is the excitation energy. Equation (20) is valid at zero temperature and for $\omega > 0$. Results for $\omega < 0$ can be easily obtained by noting that the imaginary part of the linear-response function we are interested in is antisymmetric² under the exchange $\omega \leftrightarrow -\omega$. Finally, the “rotated” longitudinal current operator $\hat{q} \cdot \hat{j}'_q$ can be expanded in a power series of the form

$$\hat{q} \cdot \hat{j}'_q = \hat{q} \cdot \hat{j}_q + \hat{q} \cdot \hat{j}_{1,q} + \hat{q} \cdot \hat{j}_{2,q} + \dots, \quad (21)$$

where, for example,

$$\hat{q} \cdot \hat{j}_{1,q} = [i\hat{F}_1, \hat{q} \cdot \hat{j}_q], \quad (22)$$

$$\hat{q} \cdot \hat{j}_{2,q} = [i\hat{F}_2, \hat{q} \cdot \hat{j}_q] + \frac{1}{2}[i\hat{F}_1, [i\hat{F}_1, \hat{q} \cdot \hat{j}_q]], \quad (23)$$

etc. Here $\hat{j}_{n,q}$ is the contribution of order n (in the strength of Coulomb interactions) to the “rotated” current operator \hat{j}'_q .

The key idea now is to realize that the calculation of $\text{Im}[\chi_{jj}^{(L)}(q, \omega)]$ to *second* order in the strength of e-e interaction requires only the knowledge of the transformed current-density operator \hat{j}'_q to *first* order, i.e., $\hat{j}'_q = \hat{j}_q + \hat{j}_{1,q}$. The untransformed current operator \hat{j}_q is indeed a one-particle operator and can only excite single particle-hole pairs which

do not contribute to the plasmon lifetime for $v_F q \ll \omega \ll 2\varepsilon_F$. From this we see that

$$\sum_m \langle 0 | \hat{q} \cdot \hat{j}_q | m \rangle \langle m | \hat{q} \cdot \hat{j}_{-q} | 0 \rangle \delta(\omega - \omega_{m0}) = 0 \quad (24)$$

and that

$$\sum_m \langle 0 | \hat{q} \cdot \hat{j}_q | m \rangle \langle m | \hat{q} \cdot \hat{j}_{1,-q} | 0 \rangle \delta(\omega - \omega_{m0}) = 0 \quad (25)$$

since $\hat{q} \cdot \hat{j}_q$ can excite only single electron-hole pairs, whose phase space is bounded inside the RPA particle-hole continuum. For the same reason, contributions to the Lehmann sum in Eq. (20) of the form

$$\sum_m \langle 0 | \hat{q} \cdot \hat{j}_q | m \rangle \langle m | \hat{q} \cdot \hat{j}_{n,-q} | 0 \rangle \delta(\omega - \omega_{m0}) \quad (26)$$

for all $n = 0, 1, 2, \dots$ vanish outside the single-particle electron-hole continuum. Thus, to *second order* in the strength of Coulomb interactions, and for $v_F q \ll \omega \ll 2\varepsilon_F$, Eq. (20) reduces to

$$\begin{aligned} \text{Im}[\chi_{jj}^{(L)}(q, \omega)] \\ = -\pi \sum_m \langle 0 | \hat{q} \cdot \hat{j}_{1,q} | m \rangle \langle m | \hat{q} \cdot \hat{j}_{1,-q} | 0 \rangle \delta(\omega - \omega_{m0}). \end{aligned} \quad (27)$$

V. CALCULATION OF \hat{F}_1 AND $\hat{j}_{1,q}$

We now proceed to calculate the operator \hat{F}_1 . We introduce

$$\mathbf{k}_{\pm} \equiv \mathbf{k} \pm \frac{1}{2}\mathbf{q}', \quad (28)$$

$$\mathbf{k}'_{\pm} \equiv \mathbf{k}' \pm \frac{1}{2}\mathbf{q}', \quad (29)$$

and the following ansatz for the operator \hat{F}_1 :

$$\begin{aligned} i\hat{F}_1 &\equiv \frac{1}{2} \sum_{q'} v_{q'} \sum_{\mathbf{k}, \mathbf{k}'} \sum_{\lambda, \lambda', \mu, \mu'} \mathcal{M}_{\lambda, \lambda', \mu, \mu'}(\mathbf{k}, \mathbf{k}', \mathbf{q}') \\ &\times c_{\mathbf{k}_-, \lambda}^{\dagger} c_{\mathbf{k}_+, \lambda'} c_{\mathbf{k}'_+, \mu}^{\dagger} c_{\mathbf{k}'_-, \mu'}. \end{aligned} \quad (30)$$

We determine $\mathcal{M}_{\lambda, \lambda', \mu, \mu'}(\mathbf{k}, \mathbf{k}', \mathbf{q}')$ to satisfy the first identity in Eq. (19).

The commutator between the noninteracting Hamiltonian $\hat{\mathcal{H}}_0$ and $i\hat{F}_1$ reads

$$\begin{aligned} [\hat{\mathcal{H}}_0, i\hat{F}_1] &= \frac{1}{2} \sum_{q'} v_{q'} \sum_{\mathbf{k}, \mathbf{k}'} \sum_{\lambda, \lambda', \mu, \mu'} \mathcal{M}_{\lambda, \lambda', \mu, \mu'}(\mathbf{k}, \mathbf{k}', \mathbf{q}') \\ &\times (\varepsilon_{\mathbf{k}_-, \lambda} - \varepsilon_{\mathbf{k}_+, \lambda'} + \varepsilon_{\mathbf{k}'_+, \mu} - \varepsilon_{\mathbf{k}'_-, \mu'}) \\ &\times c_{\mathbf{k}_-, \lambda}^{\dagger} c_{\mathbf{k}_+, \lambda'} c_{\mathbf{k}'_+, \mu}^{\dagger} c_{\mathbf{k}'_-, \mu'}. \end{aligned} \quad (31)$$

Comparing the previous equation with Eq. (5) we immediately find

$$\mathcal{M}_{\lambda, \lambda', \mu, \mu'}(\mathbf{k}, \mathbf{k}', \mathbf{q}') = \frac{\mathcal{D}_{\lambda\lambda'}(\mathbf{k}_-, \mathbf{k}_+) \mathcal{D}_{\mu\mu'}(\mathbf{k}'_+, \mathbf{k}'_-)}{\varepsilon_{\mathbf{k}_-, \lambda} - \varepsilon_{\mathbf{k}_+, \lambda'} + \varepsilon_{\mathbf{k}'_+, \mu} - \varepsilon_{\mathbf{k}'_-, \mu'}}. \quad (32)$$

The operator $\hat{j}_{1,q}$ can be easily obtained by utilizing Eq. (22). After some straightforward but lengthy algebraic

manipulations we obtain

$$\begin{aligned} \hat{q} \cdot \hat{j}_{1,q} = & \frac{1}{2} \sum_{\substack{q' \\ k, k'}} v_{q'} \sum_{\substack{\lambda, \lambda' \\ \mu, \mu', \rho}} \left\{ \hat{c}_{k_-, \lambda}^\dagger \hat{c}_{k_+, \lambda'} \hat{c}_{k_+ - q/2, \mu}^\dagger \hat{c}_{k_- + q/2, \mu'} \left[\mathcal{M}_{\lambda, \lambda', \mu, \rho} \left(\mathbf{k}, \mathbf{k}' - \frac{\mathbf{q}}{2}, \mathbf{q}' \right) \mathcal{S}_{\rho\mu'}^{(x)} \left(\mathbf{k}' - \frac{\mathbf{q}}{2}, \mathbf{k}' + \frac{\mathbf{q}}{2} \right) \right. \right. \\ & - \mathcal{M}_{\lambda, \lambda', \rho, \mu'} \left(\mathbf{k}, \mathbf{k}' + \frac{\mathbf{q}}{2}, \mathbf{q}' \right) \mathcal{S}_{\mu\rho}^{(x)} \left(\mathbf{k}' + \frac{\mathbf{q}}{2}, \mathbf{k}' + \frac{\mathbf{q}}{2} \right) \left. \right] + \hat{c}_{k_- - q/2, \lambda}^\dagger \hat{c}_{k_+ + q/2, \lambda'} \hat{c}_{k_+, \mu}^\dagger \hat{c}_{k_-, \mu'} \\ & \times \left[\mathcal{M}_{\lambda, \rho, \mu, \mu'} \left(\mathbf{k} - \frac{\mathbf{q}}{2}, \mathbf{k}', \mathbf{q}' \right) \mathcal{S}_{\rho\lambda'}^{(x)} \left(\mathbf{k}_+ - \frac{\mathbf{q}}{2}, \mathbf{k}_+ + \frac{\mathbf{q}}{2} \right) - \mathcal{M}_{\rho, \lambda', \mu, \mu'} \left(\mathbf{k} + \frac{\mathbf{q}}{2}, \mathbf{k}', \mathbf{q}' \right) \mathcal{S}_{\lambda\rho}^{(x)} \left(\mathbf{k}_- - \frac{\mathbf{q}}{2}, \mathbf{k}_- + \frac{\mathbf{q}}{2} \right) \right] \left. \right\}. \quad (33) \end{aligned}$$

In writing Eq. (33) we have used that

$$\mathbf{f}_{\mathbf{k}+q/2} - \mathbf{f}_{\mathbf{k}-q/2} \rightarrow v_F \mathbf{q}, \quad (34)$$

when \mathbf{k} is close to the \mathbf{K} point of the BZ. Equation (34) is exact in the low-energy MDF continuum limit, which will be taken momentarily. The same limit restores rotational invariance: We therefore have the liberty of fixing the direction of the wave vector \mathbf{q} arbitrarily. In Eq. (33) we have taken $\mathbf{q} = q \hat{x}$, without loss of generality.

We remind the reader that our goal is not to calculate $\hat{j}_{1,q}$ *per se*, but to calculate $\text{Im}[\chi_{jj}^{(L)}(q, \omega)]$ as from Eq. (27). The latter contains only matrix elements of $\hat{q} \cdot \hat{j}_{1,q}$ between the

states $|0\rangle$ and $|m\rangle$, multiplied by the factor $\delta(\omega + \omega_{m0})$. This property can be used to simplify the energy denominators inside all the “ \mathcal{M} functions” that appear on the right-hand side of Eq. (33). Indeed, the δ function constrains the energy difference between initial and final states: For the first term on the right-hand side of Eq. (33) it must be

$$\omega = \varepsilon_{k_-, \lambda} - \varepsilon_{k_+, \lambda'} + \varepsilon_{k_+ - q/2, \mu} - \varepsilon_{k_- + q/2, \mu'}, \quad (35)$$

while for the second term

$$\omega = \varepsilon_{k_- - q/2, \lambda} - \varepsilon_{k_+ + q/2, \lambda'} + \varepsilon_{k_+, \mu} - \varepsilon_{k_-, \mu'}. \quad (36)$$

Using Eqs. (35) and (36) in Eq. (33) we get

$$\begin{aligned} \mathcal{M}_{\lambda, \lambda', \mu, \rho} \left(\mathbf{k}, \mathbf{k}' - \frac{\mathbf{q}}{2}, \mathbf{q}' \right) &= \frac{\mathcal{D}_{\lambda\lambda'}(\mathbf{k}_-, \mathbf{k}_+) \mathcal{D}_{\mu\rho}(\mathbf{k}'_+ - q/2, \mathbf{k}'_- - q/2)}{\varepsilon_{k_-, \lambda} - \varepsilon_{k_+, \lambda'} + \varepsilon_{k_+ - q/2, \mu} - \varepsilon_{k_- - q/2, \rho}} = \frac{\mathcal{D}_{\lambda\lambda'}(\mathbf{k}_-, \mathbf{k}_+) \mathcal{D}_{\mu\rho}(\mathbf{k}'_+ - q/2, \mathbf{k}'_- - q/2)}{\omega + \varepsilon_{k_+ + q/2, \mu'} - \varepsilon_{k_- - q/2, \rho}}, \\ \mathcal{M}_{\lambda, \lambda', \rho, \mu'} \left(\mathbf{k}, \mathbf{k}' + \frac{\mathbf{q}}{2}, \mathbf{q}' \right) &= \frac{\mathcal{D}_{\lambda\lambda'}(\mathbf{k}_-, \mathbf{k}_+) \mathcal{D}_{\rho\mu'}(\mathbf{k}'_+ + q/2, \mathbf{k}'_- + q/2)}{\varepsilon_{k_-, \lambda} - \varepsilon_{k_+, \lambda'} + \varepsilon_{k_+ + q/2, \rho} - \varepsilon_{k_- + q/2, \mu'}} = \frac{\mathcal{D}_{\lambda\lambda'}(\mathbf{k}_-, \mathbf{k}_+) \mathcal{D}_{\rho\mu'}(\mathbf{k}'_+ + q/2, \mathbf{k}'_- + q/2)}{\omega + \varepsilon_{k_+ + q/2, \rho} - \varepsilon_{k_- - q/2, \mu'}}, \\ \mathcal{M}_{\lambda, \rho, \mu, \mu'} \left(\mathbf{k} - \frac{\mathbf{q}}{2}, \mathbf{k}', \mathbf{q}' \right) &= \frac{\mathcal{D}_{\lambda\rho}(\mathbf{k}_- - q/2, \mathbf{k}_+ - q/2) \mathcal{D}_{\mu\mu'}(\mathbf{k}'_+, \mathbf{k}'_-)}{\varepsilon_{k_- - q/2, \lambda} - \varepsilon_{k_+ - q/2, \rho} + \varepsilon_{k_+, \mu} - \varepsilon_{k_-, \mu'}} = \frac{\mathcal{D}_{\lambda\rho}(\mathbf{k}_- - q/2, \mathbf{k}_+ - q/2) \mathcal{D}_{\mu\mu'}(\mathbf{k}'_+, \mathbf{k}'_-)}{\omega + \varepsilon_{k_+ + q/2, \lambda'} - \varepsilon_{k_+ - q/2, \rho}}, \\ \mathcal{M}_{\rho, \lambda', \mu, \mu'} \left(\mathbf{k} + \frac{\mathbf{q}}{2}, \mathbf{k}', \mathbf{q}' \right) &= \frac{\mathcal{D}_{\rho\lambda'}(\mathbf{k}_- + q/2, \mathbf{k}_+ + q/2) \mathcal{D}_{\mu\mu'}(\mathbf{k}'_+, \mathbf{k}'_-)}{\varepsilon_{k_- + q/2, \rho} - \varepsilon_{k_+ + q/2, \lambda'} + \varepsilon_{k_+, \mu} - \varepsilon_{k_-, \mu'}} = \frac{\mathcal{D}_{\rho\lambda'}(\mathbf{k}_- + q/2, \mathbf{k}_+ + q/2) \mathcal{D}_{\mu\mu'}(\mathbf{k}'_+, \mathbf{k}'_-)}{\omega + \varepsilon_{k_- + q/2, \rho} - \varepsilon_{k_- - q/2, \lambda}} \end{aligned} \quad (37)$$

which allow us to rewrite

$$\hat{q} \cdot \hat{j}_{1,q} = \frac{1}{2} \sum_{q'} v_{q'} [\hat{\Upsilon}_{q, q'} \hat{n}_{-q'} + \hat{n}_{q'} \hat{\Upsilon}_{q, -q'}], \quad (38)$$

where

$$\hat{\Upsilon}_{q, q'} = \sum_{k, \lambda, \lambda'} \hat{c}_{k_- - q/2, \lambda}^\dagger [\hat{q} \cdot \mathbf{M}_{\lambda, \lambda'}(\mathbf{k}, \mathbf{q}', \mathbf{q})] \hat{c}_{k_+ + q/2, \lambda'}, \quad (39)$$

with

$$\hat{q} \cdot \mathbf{M}_{\lambda, \lambda'}(\mathbf{k}, \mathbf{q}', \mathbf{q}) \equiv \sum_{\rho} \left[\frac{\mathcal{D}_{\lambda\rho}(\mathbf{k}_- - \frac{\mathbf{q}}{2}, \mathbf{k}_+ - \frac{\mathbf{q}}{2}) \mathcal{S}_{\rho\lambda'}^{(x)}(\mathbf{k}_+ - \frac{\mathbf{q}}{2}, \mathbf{k}_+ + \frac{\mathbf{q}}{2})}{\omega + \varepsilon_{k_+ + q/2, \lambda'} - \varepsilon_{k_+ - q/2, \rho}} - \frac{\mathcal{S}_{\lambda\rho}^{(x)}(\mathbf{k}_- - \frac{\mathbf{q}}{2}, \mathbf{k}_- + \frac{\mathbf{q}}{2}) \mathcal{D}_{\rho\lambda'}(\mathbf{k}_- + \frac{\mathbf{q}}{2}, \mathbf{k}_+ + \frac{\mathbf{q}}{2})}{\omega + \varepsilon_{k_- + q/2, \rho} - \varepsilon_{k_- - q/2, \lambda}} \right]. \quad (40)$$

We stress that Eqs. (38)–(40) are valid only for their use in Eq. (27).

VI. REDUCTION OF $\hat{\Upsilon}_{q, q'}$ TO A CURRENT-LIKE OPERATOR

We now proceed to approximate the microscopic expression of the operator $\hat{\Upsilon}_{q, q'}$ in Eqs. (39) and (40) by taking the limits $q \rightarrow 0$ and $v_F q \ll \omega \ll 2\varepsilon_F$. We will try to slowly guide the reader through the many steps of this lengthy process.

To begin with, in the long-wavelength $q \rightarrow 0$ limit we can write

$$\frac{1}{\omega + \varepsilon_{k_{\pm}+q/2,\lambda} - \varepsilon_{k_{\pm}-q/2,\rho}} \rightarrow \delta_{\lambda,\rho} \left[\frac{1}{\omega} - \frac{q}{\omega^2} \frac{\partial \varepsilon_{k_{\pm}}}{\partial k_x} \right] + (1 - \delta_{\lambda,\rho}) \frac{1}{\omega + 2\lambda \varepsilon_F} + O(q^2). \quad (41)$$

We then observe that in the regime of interest in this paper, i.e., $v_F q \ll \omega \ll 2\varepsilon_F$, the particle-hole states created by the operator $\hat{Y}_{q,q'}$ are energetically close to the Fermi energy. The band indices on λ, λ' on the right-hand side of Eq. (40) are therefore constrained to take the following values: $\lambda = \lambda' = +1$ (recall that $\varepsilon_F > 0$).

Note that the ‘‘virtual state’’ ρ , over which the sum on the right-hand side of Eq. (40) runs, can be either in conduction ($\rho = +1$) or valence ($\rho = -1$) band, even though the states labeled by the band indices λ and λ' are bound to the Fermi surface.

We first simplify Eqs. (39) and (40) by using Eq. (41). We are naturally led to define

$$\begin{aligned} \hat{q} \cdot \mathbf{M}_{\text{intra}}(\mathbf{k}, \mathbf{q}', \mathbf{q}) \equiv \hat{q} \cdot \mathbf{M}_{\lambda,\lambda'}(\mathbf{k}, \mathbf{q}', \mathbf{q})|_{\rho=+1} &= \cos\left(\frac{\theta_{k_- - q/2} - \theta_{k_+ - q/2}}{2}\right) \cos(\theta_{k_+}) \left[\frac{1}{\omega} - \frac{v_F q}{\omega^2} \cos(\theta_{k_+}) \right] \\ &\quad - \cos\left(\frac{\theta_{k_- + q/2} - \theta_{k_+ + q/2}}{2}\right) \cos(\theta_{k_-}) \left[\frac{1}{\omega} - \frac{v_F q}{\omega^2} \cos(\theta_{k_-}) \right] + O(q^2) \end{aligned} \quad (42)$$

and

$$\begin{aligned} \hat{q} \cdot \mathbf{M}_{\text{inter}}(\mathbf{k}, \mathbf{q}', \mathbf{q}) \equiv \hat{q} \cdot \mathbf{M}_{\lambda,\lambda'}(\mathbf{k}, \mathbf{q}', \mathbf{q})|_{\rho=-1} &= -\frac{1}{2\varepsilon_F} \sin\left(\frac{\theta_{k_- - q/2} - \theta_{k_+ - q/2}}{2}\right) \sin\left(\frac{\theta_{k_+ - q/2} + \theta_{k_+ + q/2}}{2}\right) \\ &\quad + \frac{1}{2\varepsilon_F} \sin\left(\frac{\theta_{k_- + q/2} - \theta_{k_+ + q/2}}{2}\right) \sin\left(\frac{\theta_{k_- - q/2} + \theta_{k_- + q/2}}{2}\right) + O(q^2) \end{aligned} \quad (43)$$

so that in the limit $v_F q \ll \omega \ll 2\varepsilon_F$ we have

$$\hat{q} \cdot \mathbf{M}_{\lambda,\lambda'}(\mathbf{k}, \mathbf{q}', \mathbf{q}) = \hat{q} \cdot \mathbf{M}_{\text{intra}}(\mathbf{k}, \mathbf{q}', \mathbf{q}) + \hat{q} \cdot \mathbf{M}_{\text{inter}}(\mathbf{k}, \mathbf{q}', \mathbf{q}). \quad (44)$$

In writing Eq. (43) we have taken the limit $\omega \rightarrow 0$ in the second term on the right-hand side of Eq. (41). Moreover, in obtaining Eq. (42) we have used that

$$\cos\left(\frac{\theta_{k_{\pm} - q/2} + \theta_{k_{\pm} + q/2}}{2}\right) = \cos(\theta_{k_{\pm}}) + O(q^2) \quad (45)$$

and

$$\frac{\partial \varepsilon_{k_{\pm},\lambda}}{\partial k_x} \rightarrow \lambda v_F \cos(\theta_{k_{\pm}}). \quad (46)$$

The last equation becomes exact for \mathbf{k} close to the \mathbf{K} point of the BZ and therefore in the low-energy MDF limit.

Clearly we can carry out further approximations, relying on the fact that we are interested in the low-energy MDF limit. Equation (42) can be further simplified by noting that

$$\cos\left(\frac{\theta_{k_{\pm} \pm q/2} - \theta_{k_{\pm} \pm q/2}}{2}\right) = \cos\left(\frac{\theta_{k_- - q/2} - \theta_{k_+ + q/2}}{2}\right) - \frac{q}{2} \sin\left(\frac{\theta_{k_-} - \theta_{k_+}}{2}\right) \frac{\partial \theta_{k_{\mp}}}{\partial k_x} + O(q^2), \quad (47)$$

which leads to

$$\begin{aligned} \hat{q} \cdot \mathbf{M}_{\text{intra}} &= \frac{\cos(\theta_{k_+}) - \cos(\theta_{k_-})}{\omega} \cos\left(\frac{\theta_{k_- - q/2} - \theta_{k_+ + q/2}}{2}\right) + \frac{v_F q}{\omega^2} [\cos^2(\theta_{k_-}) - \cos^2(\theta_{k_+})] \cos\left(\frac{\theta_{k_-} - \theta_{k_+}}{2}\right) \\ &\quad + \frac{q}{2\omega} \frac{\partial [\sin(\theta_{k_-}) - \sin(\theta_{k_+})]}{\partial k_x} \sin\left(\frac{\theta_{k_-} - \theta_{k_+}}{2}\right) + O(q^2). \end{aligned} \quad (48)$$

In the first term on the right-hand side of Eq. (48) we can approximate

$$\cos(\theta_{k_+}) - \cos(\theta_{k_-}) \rightarrow \frac{q'_x}{k_F}, \quad (49)$$

while the second term on the right-hand side of Eq. (48) becomes

$$[\cos^2(\theta_{k_-}) - \cos^2(\theta_{k_+})] \cos\left(\frac{\theta_{k_-} - \theta_{k_+}}{2}\right) \rightarrow -2 \frac{q'_x}{k_F} \left(1 - \frac{q'^2}{4k_F^2}\right) \cos\left(\frac{\theta_{k_-} + \theta_{k_+}}{2}\right). \quad (50)$$

Finally, the derivative in the third term on the right-hand side of Eq. (48) reduces to

$$\frac{\partial [\sin(\theta_{k_-}) - \sin(\theta_{k_+})]}{\partial k_x} \rightarrow -\frac{\partial (q'_y/k_F)}{\partial k_x} = 0. \quad (51)$$

Introducing Eq. (48), approximated according to Eqs. (49)–(51), back into Eq. (39) we get the “intra-band” contribution to the operator $\hat{\Upsilon}_{q,q'}$, which reads

$$\hat{\Upsilon}_{q,q'}^{(\text{intra})} = \left[\frac{v_F q'_x}{k_F \omega} \hat{n}_{q+q'} - 2 \frac{v_F q_x q'_x}{\omega^2 k_F} \left(1 - \frac{q'^2}{4k_F^2} \right) j_{q',x} \right] + O(q^2). \quad (52)$$

We remind the reader that we have taken $\mathbf{q} = q\hat{x}$ without loss of generality. Here we used that $\hat{\mathbf{j}}_q = v_F \hat{\sigma}_q$ close to the \mathbf{K} point of the BZ.

We now consider Eq. (43). Steps similar to what summarized above for the intra-band contribution to $\hat{\Upsilon}_{q,q'}$ yield

$$\begin{aligned} \hat{\mathbf{q}} \cdot \mathbf{M}_{\text{inter}} &= \frac{1}{2\varepsilon_F} [\sin(\theta_{k_-}) - \sin(\theta_{k_+})] \sin\left(\frac{\theta_{k_-} - \theta_{k_+}}{2}\right) \\ &= \frac{1}{\varepsilon_F} \sin^2\left(\frac{\theta_{k_-} - \theta_{k_+}}{2}\right) \cos\left(\frac{\theta_{k_-} + \theta_{k_+}}{2}\right) \\ &= \frac{q'^2}{4v_F k_F^3} \mathcal{S}_{\lambda\lambda'}^{(x)}(\mathbf{k}_-, \mathbf{k}_+). \end{aligned} \quad (53)$$

Once Eq. (53) is introduced into Eq. (39), it gives the “inter-band” contribution to the operator $\hat{\Upsilon}_{q,q'}$, i.e.,

$$\hat{\Upsilon}_{q,q'}^{(\text{inter})} = \frac{q'^2}{4v_F k_F^3} j_{q',x} + O(q^2). \quad (54)$$

Again we used the fact that $\hat{\mathbf{j}}_q = v_F \hat{\sigma}_q$ close to the \mathbf{K} point of the BZ.

Summing Eqs. (52) and (54) we finally get

$$\hat{\Upsilon}_{q,q'} = \frac{v_F q'_x}{k_F \omega} \hat{n}_{q+q'} + \hat{\Upsilon}'_{q,q'}, \quad (55)$$

with

$$\hat{\Upsilon}'_{q,q'} = - \left[2 \frac{v_F q_x q'_x}{\omega^2 k_F} \left(1 - \frac{q'^2}{4k_F^2} \right) - \frac{q'^2}{4v_F k_F^3} \right] \hat{j}_{q',x}. \quad (56)$$

The first term on the right-hand side of Eq. (55) can be further manipulated. Indeed, when it is introduced in Eq. (38) it gives

$$\begin{aligned} &\frac{1}{2\omega k_F} \sum_{q'} v_{q'} [q'_x \hat{n}_{q+q'} \hat{n}_{-q'} - q'_x \hat{n}_{q'} \hat{n}_{q-q'}] \\ &= \frac{v_F}{2\omega k_F} \sum_{q'} \hat{n}_{q+q'} \hat{n}_{-q'} [q'_x v_{q'} - (q + q'_x) v_{q+q'}] \\ &\rightarrow \frac{v_F q}{2\omega k_F} \sum_{q'} v_{q'} \left(\frac{q'_x}{q'^2} - 1 \right) \hat{n}_{q'} \hat{n}_{-q'} + O(q^2). \end{aligned} \quad (57)$$

Here we performed the shift $q' \rightarrow q + q'$ in the term proportional to $\hat{n}_{q'} \hat{n}_{q-q'}$ and we took the small- q limit in the last line of Eq. (57). Finally, using the continuity equation

$$\omega \hat{n}_{q'} \hat{n}_{-q'} = -q' \cdot \hat{\mathbf{j}}_{q'} \hat{n}_{-q'} + \hat{n}_{q'} q' \cdot \hat{\mathbf{j}}_{-q'}, \quad (58)$$

it is possible to redefine the operator in Eq. (55) as

$$\begin{aligned} \hat{\Upsilon}_{q,q'} &= \sum_{\alpha=x,y} \left\{ \frac{v_F q_x}{\omega^2} \left[\frac{q'_y}{q'^2} \frac{q'_\alpha}{k_F} - 2 \frac{q'_x}{k_F} \left(1 - \frac{q'^2}{4k_F^2} \right) \delta_{\alpha,x} \right] \right. \\ &\quad \left. + \frac{q'^2}{4v_F k_F^3} \delta_{\alpha,x} \right\} \hat{j}_{q',\alpha} \equiv \sum_{\alpha=x,y} \Gamma_\alpha(\mathbf{q}, \mathbf{q}') \hat{j}_{q',\alpha}. \end{aligned} \quad (59)$$

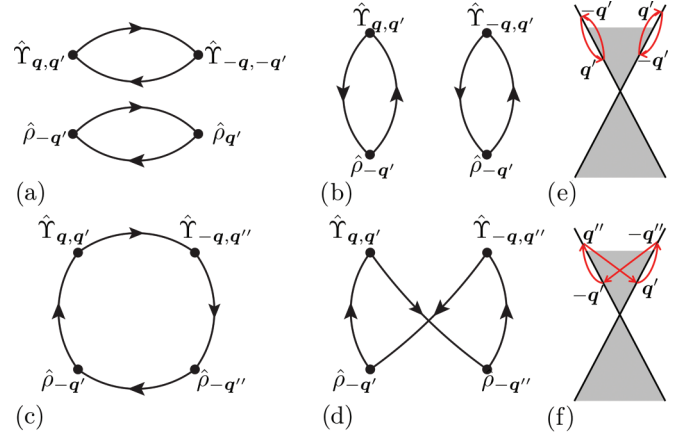


FIG. 2. (Color online) (a)–(d) Some of the diagrams that contribute to the noninteracting two-particle response function. The diagrams in (a) and (b) are the only two that contribute in the large- N_f limit. (c) and (d) Two nondisconnected diagrams which differ from each other for the order of the external vertices. (e) [(f)] depicts the excitations that are responsible for the plasmon damping in (a) and (b) [(c) and (d)].

The main differences between Eq. (59) and the corresponding expression that can be found for a 2DEG (see Appendix A) are: (i) the factor $1 - q'^2/(4k_F^2)$, which is due to the chirality of the MDF eigenstates and suppresses backscattering at the Fermi surface, and (ii) the last term in curly brackets, which is finite even in the long-wavelength $q \rightarrow 0$ limit. As to the former, we observe [see also Eq. (39)] that in the limit of $q \rightarrow 0$ q' is the total momentum of the electron-hole pair created by $\hat{\Upsilon}_{q,q'}$. Such excitations are weighted by the chirality factor $1 - \cos(\varphi_{k_-} - \varphi_{k_+})$ (recall that $\lambda = \lambda' = +$), which becomes $1 - q'^2/(4k_F^2)$ when all momenta are restricted at the Fermi surface. Note that this factor suppresses backscattering, i.e., the creation of a particle-hole pair with opposite momenta ($q' = 2k_F$). The last term in curly brackets which is finite even for $q \rightarrow 0$ is instead due to the two-band nature of graphene, which opens the possibility of a *virtual* state in valence band even though the real states labeled by the band indices λ, λ' are at the Fermi energy in conduction band. More details on the comparison between graphene and an ordinary 2DEG are presented in Appendix A.

VII. LARGE- N_f APPROXIMATION FOR THE DENSITY-DENSITY RESPONSE FUNCTION

After the change of variables $q' \rightarrow -q'$ in the second term on the right-hand side of Eq. (38), the latter can be rewritten as $\mathbf{q} \cdot \hat{\mathbf{j}}_{1,q} = \sum_{q'} v_{q'} \hat{\Upsilon}_{q,q'} \hat{n}_{-q'}$. A major simplification is suggested by the analysis of the Feynman graphs contributing to the noninteracting spectrum of $\hat{\mathbf{q}} \cdot \hat{\mathbf{j}}_{1,q}$. Some of these are shown in Figs. 2(a)–2(d). Because $\hat{\mathbf{j}}_{1,q}$ is a two-particle operator, these diagrams have *four* vertices, one for each creation-annihilation pair. We see that the disconnected graphs contain *two* independent sums over the number N_f of fermion flavors, whereas the connected ones contain only one such sum. We conclude that the disconnected graphs dominate in the large- N_f limit. The final formula for the density-density response function, which is exact to second order in e-e

interactions and in the large- N_f limit, is

$$\begin{aligned} \text{Im}[\chi_{nn}(q, \omega)] = & -\frac{q^2}{\omega^2} \sum_{\alpha, \beta=x, y} \int \frac{d^2 q'}{(2\pi)^2} v_{q'}^2 \int_0^\omega \frac{d\omega'}{\pi} \{ \Gamma_\alpha(\mathbf{q}, \mathbf{q}') \Gamma_\beta(-\mathbf{q}, -\mathbf{q}') \text{Im}[\chi_{nn}^{(0)}(q', \omega')] \text{Im}[\chi_{j_\alpha j_\beta}^{(0)}(\mathbf{q}', \omega - \omega')] \\ & + \Gamma_\alpha(\mathbf{q}, \mathbf{q}') \Gamma_\beta(-\mathbf{q}, \mathbf{q}') \text{Im}[\chi_{nj_\alpha}^{(0)}(-\mathbf{q}', \omega')] \text{Im}[\chi_{nj_\beta}^{(0)}(\mathbf{q}', \omega - \omega')] \}. \end{aligned} \quad (60)$$

In this equation $\chi_{nn}^{(0)}(q, \omega)$, $\chi_{j_\alpha j_\beta}^{(0)}(\mathbf{q}, \omega)$, and $\chi_{nj_\alpha}^{(0)}(\mathbf{q}, \omega)$ are the *noninteracting* density-density, current-current, and density-current response functions of a 2D gas of MDFs. The quantities $\{\Gamma_\alpha(\mathbf{q}, \mathbf{q}'), \alpha = x, y\}$ are defined in Eq. (59). We stress that the *imaginary* parts of the three linear-response functions $\chi_{nn}^{(0)}(q, \omega)$, $\chi_{j_\alpha j_\beta}^{(0)}(\mathbf{q}, \omega)$, and $\chi_{nj_\alpha}^{(0)}(\mathbf{q}, \omega)$ do not depend on any ultraviolet cutoff in the low-energy MDF limit. Moreover, since in the limit of $\omega \rightarrow 0$ the integral over q' is naturally restricted to $0 \leq q' \leq 2k_F$, no ultraviolet regularization is needed in Eq. (60). The only pathology of the integral in Eq. (60) appears in the infrared $q' \rightarrow 0$ limit, due to the $1/q'$ singularity of the Coulomb potential $v_{q'}$. This problem is cured by screening, as we will further discuss below.

Equation (60) is the main result of this section. Note that in the large- N_f limit the second-order expression for the imaginary part of the density-density response function in Eq. (60) has the appealing form of a convolution of two single-particle spectra (with the current operator decoupled from the density operator). The physical interpretation of Eq. (60) is the following. At long wavelengths and to the lowest nonvanishing order of perturbation theory, a plasmon decays by emitting two electron-hole pairs [see Figs. 2(e) and 2(f)]. Each of the Kubo products on the right-hand side of Eq. (60) describes the rate of generation of a single electron-hole pair. The spectral weight associated with the excitation of two particle-hole pairs with opposite momenta and given total energy ω is proportional to their convolution.

In passing, we mention that Eq. (60) can also be obtained by means of “brute-force” many-body diagrammatic perturbation theory when only diagrams of second order in the strength of e-e interactions and containing two bubbles (i.e., a factor N_f^2) are retained. This statement is proven in Appendix B, where, for the sake of simplicity, we have reported diagrammatic calculations for the case of an ordinary 2DEG only.

We now sketch how to make analytical progress in the evaluation of $\text{Im}[\chi_{nn}(q, \omega)]$ as from Eq. (60).

The integrals in Eq. (60) can be carried out analytically with the help of known formulas for the response functions.⁵ We

first observe that in the low-energy MDF limit the system is translationally and rotationally invariant. The current-current linear-response function $\chi_{j_\alpha j_\beta}^{(0)}(\mathbf{q}, \omega)$ is a rank-2 tensor that can be therefore decomposed according to²

$$\chi_{j_\alpha j_\beta}^{(0)}(\mathbf{q}, \omega) = \chi_{jj}^{(0,L)}(q, \omega) \frac{q_\alpha q_\beta}{q^2} + \chi_{jj}^{(0,T)}(q, \omega) \left(\delta_{\alpha, \beta} - \frac{q_\alpha q_\beta}{q^2} \right), \quad (61)$$

where $\chi_{jj}^{(0,L)}(q, \omega)$ and $\chi_{jj}^{(0,T)}(q, \omega)$ are the noninteracting longitudinal and transverse current-current response functions, respectively.

In the limit $\omega \rightarrow 0$ we can expand the imaginary part of each response function $\chi_{nn}^{(0)}$, $\chi_{nj_\alpha}^{(0)}$, $\chi_{jj}^{(0,L)}$, and $\chi_{jj}^{(0,T)}$ in a power series of ω' , $\omega - \omega'$ and retain only the leading order of this expansion. The leading contribution to $\text{Im}[\chi_{nn}(q, \omega)]$ in powers of ω in the limit $\omega \rightarrow 0$ can be extracted from the following asymptotic formulas:

$$\lim_{\omega' \rightarrow 0} \text{Im}[\chi_{nn}^{(0)}(q', \omega')] = -N_f \frac{\sqrt{4k_F^2 - q'^2}}{2q'} \frac{\omega'}{2\pi v_F^2} \quad (62)$$

and

$$\lim_{\omega' \rightarrow 0} \text{Im}[\chi_{jj}^{(0,T)}(q', \omega')] = -N_f \frac{2k_F}{q' \sqrt{4k_F^2 - q'^2}} \frac{\omega'}{2\pi v_F}. \quad (63)$$

The imaginary parts of density-current and longitudinal current-current response functions scale with higher powers of ω' .

VIII. RESULTS AND DISCUSSION

A. The DP damping rate

Substituting Eqs. (62) and (63) in Eq. (60) we finally get

$$\text{Im}[\chi_{nn}(q, \omega)] = -\frac{q}{2\pi v_F} \left[\mathcal{A}_{N_f}(\alpha_{ee}) \frac{v_F^3 q^3}{\omega^3} + \mathcal{B}_{N_f}(\alpha_{ee}) \frac{q\omega}{v_F k_F^2} \right], \quad (64)$$

where $\mathcal{A}_{N_f}(\alpha_{ee}) = N_f^2 \alpha_{ee}^2 f(N_f \alpha_{ee})$ and $\mathcal{B}_{N_f}(\alpha_{ee}) = N_f^2 \alpha_{ee}^2 g(N_f \alpha_{ee})$, with

$$f(x) = \frac{15x^3 - 15x^2 - 52x + 42 - 3(5x^4 - 24x^2 + 16)\text{arccoth}(1+x)}{288\pi} \quad (65)$$

and

$$g(x) = \frac{3x^2 + 3x - 2 - 3x^2(2+x)\text{arccoth}(1+x)}{96\pi(2+x)}. \quad (66)$$

We remark that Eq. (64) is valid only to leading order for $q \rightarrow 0$ and $v_F q \ll \omega \ll 2\varepsilon_F$. Equations (64)–(66) are the most important analytical results of this paper.

In Eq. (64) we have introduced the well-known dimensionless parameter (after restoring \hbar)

$$\alpha_{ee} \equiv \frac{e^2}{\hbar v_F \epsilon}, \quad (67)$$

which measures the strength of e-e interactions relative to the kinetic energy when the low-energy MDF limit is taken.^{10,11} For a flake on a typical substrate like SiO₂^{9–11} or h-BN,²⁷ $\alpha_{ee} < 1$, therefore justifying a perturbative treatment of $\hat{\mathcal{H}}_{ee}$. Only suspended samples²⁸ ($\alpha_{ee} \sim 2.2$) are formally outside the perturbative regime.

Importantly, in obtaining Eq. (64) we have used a statically screened interaction of the form

$$v_q = \frac{2\pi e^2}{\epsilon q} \frac{1}{\varepsilon_{TF}(q)}, \quad (68)$$

where $\varepsilon_{TF}(q) = 1 + q_{TF}/q$ and $q_{TF} = N_f \alpha_{ee} k_F$ is the Thomas-Fermi screening wave vector.¹¹ Static screening is fully justified since we are interested in the $\omega \rightarrow 0$ limit of Eq. (60). The dependence of $\mathcal{A}_{N_f}(\alpha_{ee})$ and $\mathcal{B}_{N_f}(\alpha_{ee})$ on α_{ee} beyond α_{ee}^2 , which is encoded into the functions $f(x)$ and $g(x)$ evaluated at $x = N_f \alpha_{ee}$, stems from the use of Eq. (68), which, as stated above, is needed to cure infrared divergences associated with the bare Coulomb potential.⁶

The first term on the right-hand side of Eq. (64)—the one controlled by the quantity $\mathcal{A}_{N_f}(\alpha_{ee})$ —can be traced back to the term in square brackets on the right-hand side of Eq. (59), which vanishes in the limit $q \rightarrow 0$. This term is analogous to what one finds in the case of an ordinary 2DEG—see Appendix A—*modulo* the factor $1 - q^2/(4k_F^2)$ which suppresses backscattering. This chirality factor yields major quantitative differences between the DP damping rate and the damping rate of a plasmon in a 2DEG (see below). The second term on the right-hand side of Eq. (64)—the one controlled by the function $\mathcal{B}_{N_f}(\alpha_{ee})$ —is instead due to the Galilean-breaking term in the second line of Eq. (59), and is therefore peculiar to graphene.

As already pointed out in Sec. II, the DP damping rate can be calculated from the usual equation² $1 - v_q \chi_{\rho\rho}[q, \omega_p(q) - i\Gamma_p(q)] = 0$, which can be expanded for $\Gamma_p(q) \ll \omega_p(q)$ to give

$$1 - v_q \text{Re}[\chi_{nn}(q, \omega_p(q))] = 0, \quad (69)$$

$$\Gamma_p(q) = \frac{\text{Im}[\chi_{nn}(q, \omega_p(q))]}{\left. \frac{\partial \text{Re}[\chi_{nn}(q, \omega)]}{\partial \omega} \right|_{\omega=\omega_p(q)}}.$$

Since $\text{Im}[\chi_{nn}(q, \omega)]$ starts already at second order in the strength α_{ee} of e-e interactions, we can take $\text{Re}[\chi_{nn}(q, \omega)] = \text{Re}[\chi_{nn}^{(0)}(q, \omega)]$ in the second of Eqs. (69). Moreover, in both Eqs. (69) we can use the RPA DP dispersion (11).

The final result for the DP damping rate can be cast (after restoring \hbar) into the following elegant form:

$$\Gamma_p(q) = \frac{\varepsilon_F}{\hbar} \mathcal{A}_{N_f}(\alpha_{ee}) \left(\frac{q}{k_F} \right)^2. \quad (70)$$

Note that only the first term on the right-hand side of Eq. (64) contributes to the DP damping rate at the lowest nonvanishing order in perturbation theory, i.e., $O(\alpha_{ee}^2)$. The term proportional

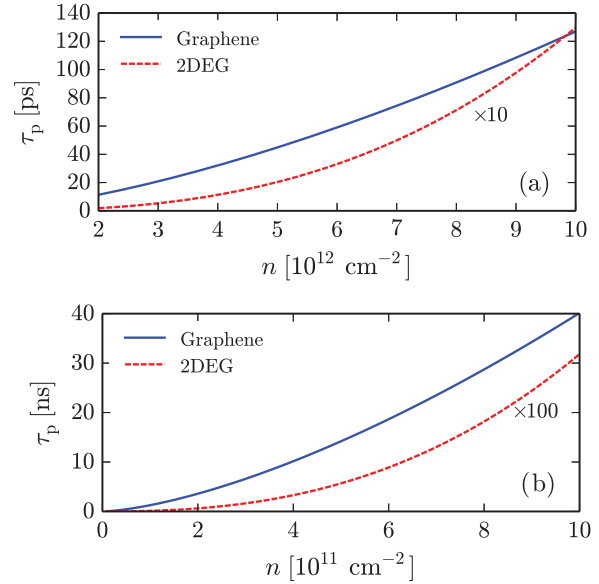


FIG. 3. (Color online) The intrinsic Dirac plasmon lifetime $\tau_p(q_1)$ is plotted as a function of electron density n and for a fixed photon energy $\hbar\omega_{ph}$. The (blue) solid line refers to $\alpha_{ee} = 0.9$. The (red) dashed line refers to a 2DEG in a GaAs quantum well. The intrinsic lifetime of a 2DEG plasmon is much shorter, at least by a factor 10: The dashed curves have been multiplied by large enhancement factors to fit into the frames of the figures. Different parts refer to different values of the photon energy: in (a) we have set $\hbar\omega_{ph} = 112$ meV corresponding to mid-infrared plasmons; in (b) $\hbar\omega_{ph} = 11.2$ meV corresponds to Terahertz plasmons. Note the difference in the scales of horizontal and vertical axes between the two parts.

to $\mathcal{B}_{N_f}(\alpha_{ee})$ gives a contribution to the DP damping rate that goes like $\mathcal{B}_{N_f}(\alpha_{ee})\omega_p^4(q)$. However, since $\omega_p(q) \propto \sqrt{\alpha_{ee}}$, such a term is $O(\alpha_{ee}^4)$ and must be neglected to be consistent with the rest of the calculation, which is correct only up to order $O(\alpha_{ee}^2)$.

In Fig. 3 we plot the DP lifetime $\tau_p(q)$ calculated from Eq. (1), where $\Gamma_p(q)$ is provided by Eq. (70). Following Ref. 15, this quantity has been plotted for q equal to the plasmon wave number $q_1/k_F = (2\alpha_{ee})^{-1}(\hbar\omega_{ph}/\varepsilon_F)^2$ for a fixed photon energy $\hbar\omega_{ph}$. As density decreases q_1/k_F increases. From this figure we clearly see that the intrinsic DP lifetime can be of the order of 20–120 ps for mid-infrared plasmons and of tens of nanoseconds for Terahertz plasmons. For the sake of comparison, in Fig. 3 we have also plotted the intrinsic lifetime of a plasmon in an ordinary 2DEG hosted in a GaAs quantum well. Clearly DPs have a much longer intrinsic lifetime than 2DEG plasmons (at least a factor 10 longer). This difference stems from the chirality factor which characterizes the electron wave functions in a graphene sheet. This factor suppresses backscattering at the Fermi surface^{9–11} therefore enhancing the DP intrinsic lifetime with respect to that of a plasmon in an ordinary 2DEG, which is calculated, for the sake of completeness, in Appendix A.

In Fig. 4 we plot the DP intrinsic inverse quality factor

$$\gamma_p(q) = 2 \frac{\Gamma_p(q)}{\omega_p(q)} = 2\sqrt{2} \frac{\mathcal{A}_{N_f}(\alpha_{ee})}{\sqrt{N_f \alpha_{ee}}} \left(\frac{q}{k_F} \right)^{3/2}, \quad (71)$$

calculated at $q = q_1$ and as a function of doping.

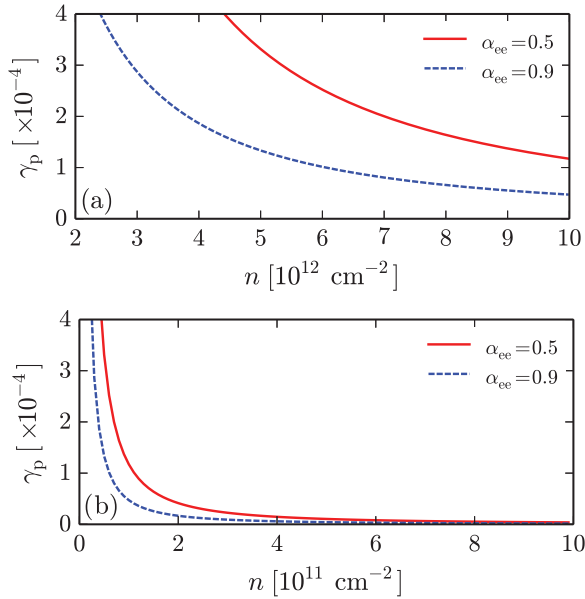


FIG. 4. (Color online) The intrinsic Dirac plasmon damping rate $\gamma_p(q_1)$ is plotted as a function of electron density n and for a fixed photon energy $\hbar\omega_{\text{ph}}$. In this figure different curves refer to different values of the graphene fine-structure constant α_{ee} . As in Fig. 3, (a) refers to mid-infrared plasmons, while (b) refers to Terahertz plasmons.

From Eq. (71) we clearly see that $\gamma_p(q_1) \propto (\hbar\omega_{\text{ph}}/\varepsilon_F)^3$. From Fig. 4(a) we note that, in the range of densities explored in Ref. 15, the dependence of γ_p on doping is weak. Although this is in agreement with Ref. 15, the numerical value we find for the DP inverse quality factor in the mid infrared ($\gamma_p \approx 10^{-4}$) is much smaller than the measured value ($\gamma_p \approx 10^{-1}$). We are therefore led to conclude that the experiments in Refs. 15 and 16 are far from the intrinsic regime where many-body effects would be dominant. Indeed, as stressed in Ref. 20, the experimental results for the DP damping rate published in Refs. 15 and 16 can be explained in terms of scattering of plasmons against charged impurities.

All the calculations described so far have been performed at zero temperature. Finite-temperature effects introduce additional damping due to the presence of thermally excited quasiparticles. We have estimated this effect using RPA²⁹ and the results are plotted in Fig. 5. We conclude that thermal effects are negligible at the typical densities of the experiments of Refs. 15 and 16, but certainly not at lower densities. The thermal broadening of DPs should therefore be taken carefully into account in any quantitative comparison between theory and experiment.

B. The background of optical absorption below the single-particle gap

We now compare our findings for the DP damping rate [Eq. (71)] with the background of optical absorption $\text{Re}[\sigma_0(\omega)]$ with

$$\sigma_0(\omega) \equiv \lim_{q \rightarrow 0} \sigma(q, \omega), \quad (72)$$

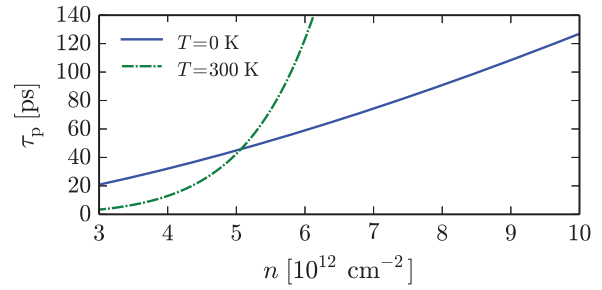


FIG. 5. (Color online) The Dirac plasmon lifetime $\tau_p(q_1)$ is plotted as a function of electron density n and for a fixed photon energy $\hbar\omega_{\text{ph}} = 112 \text{ meV}$. The (blue) solid line refers to the intrinsic plasmon lifetime calculated at $T = 0$ [the same function is plotted in Fig. 2(a)]. The (green) dash-dotted line refers to the RPA plasmon lifetime computed from the finite-temperature Lindhard function²⁹ at $T = 300 \text{ K}$. Both curves refer to $\alpha_{ee} = 0.9$.

the ac conductivity, calculated at $q = 0$ and for frequencies in the single-particle gap¹⁰ $\hbar\omega < 2\varepsilon_F$.

Making use of the relation^{1,2} $\sigma(q, \omega) = ie^2\omega\chi_{nn}(q, \omega)/q^2$ it is easy to show—see Appendix C for details—that

$$\gamma_p(q) = \frac{\text{Re}[\sigma(q, \omega)]}{\text{Im}[\sigma(q, \omega)]} \Big|_{\omega=\omega_p(q)}. \quad (73)$$

At a first sight the previous result seems to suggest that in the $q \rightarrow 0$ limit the DP damping rate γ_p is linked to the ratio of the real part to the imaginary part of the optical conductivity.¹⁵ However, this suggestion turns out to be incorrect, because the small- q behavior of $\text{Re}[\sigma(q, \omega_p(q))]$ is different from the small- q behavior of $\text{Re}[\sigma_0(\omega_p(q))]$ (see Fig. 6). To second order in α_{ee} a careful calculation shows that

$$\text{Re}[\sigma_0(\omega \ll 2\varepsilon_F/\hbar)] \equiv \sigma_1(\omega) = \frac{2\hbar^3 \mathcal{D}_0 \mathcal{B}_{N_f}(\alpha_{ee})}{\pi \varepsilon_F^3} \omega^2. \quad (74)$$

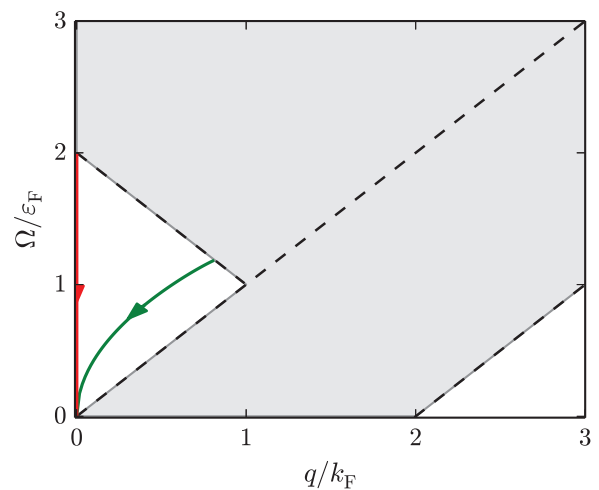


FIG. 6. (Color online) The two different ways of taking the limit $\omega \rightarrow 0$ in Eq. (60) used in this paper: Along the plasmon dispersion ($\omega \propto \sqrt{q}$ —here $\alpha_{ee} = 0.5$) and with $q = 0$ to begin with. The former is needed to obtain the inverse quality factor $\gamma_p(q)$, while the latter gives the background of optical absorption $\sigma_1(\omega)/\sigma_2(\omega)$ for $\hbar\omega \ll 2\varepsilon_F$. As shown in Sec. VIII B the two limits give different results.

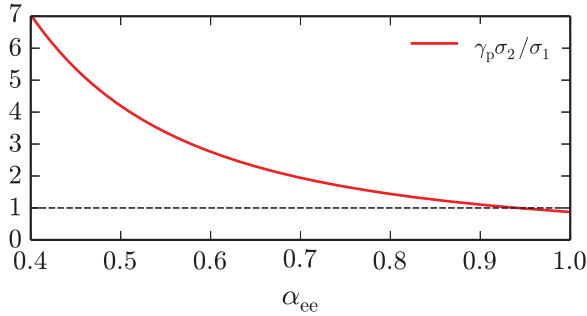


FIG. 7. (Color online) The ratio between $\gamma_p(q_1)$ and $\sigma_1(\omega)/\sigma_2(\omega)|_{\omega=\omega_{ph}}$, defined respectively in Eqs. (76) and (75). The two functions become equal for $\alpha_{ee} \simeq 0.95$.

In the same range of energies, $\text{Im}[\sigma_0(\omega)] \equiv \sigma_2(\omega) = \mathcal{D}_0/\pi\omega$. To second order in α_{ee} we therefore find

$$\frac{\sigma_1(\omega)}{\sigma_2(\omega)} \Big|_{\omega=\omega_{ph}} = 2\mathcal{B}_{N_f}(\alpha_{ee}) \left(\frac{\hbar\omega_{ph}}{\varepsilon_F} \right)^3. \quad (75)$$

Note that (i) in a Galilean-invariant system $\sigma_1(\omega)$ vanishes identically, and (ii) that in the present case this quantity depends on $\mathcal{B}_{N_f}(\alpha_{ee})$, which can be traced back to the last (Galilean-breaking) term in curly brackets on the right-hand side of Eq. (59).

Note that Eq. (75) has the same dependence on photon energy and density as Eq. (71), when the latter is evaluated at $q = q_1$, i.e.,

$$\gamma_p(q_1) = \frac{\mathcal{A}_{N_f}(\alpha_{ee})}{\sqrt{N_f}\alpha_{ee}^2} \left(\frac{\hbar\omega_{ph}}{\varepsilon_F} \right)^3. \quad (76)$$

Their functional dependence on the coupling constant α_{ee} is, however, different. In Fig. 7 we plot the ratio between Eqs. (76) and (75). We clearly see that $\gamma_p(q_1)$ is typically larger than $\sigma_1(\omega)/\sigma_2(\omega)|_{\omega=\omega_{ph}}$ at small α_{ee} , the two quantities becoming equal for $\alpha_{ee} \sim 0.95$.

IX. CONCLUSIONS

In summary, we have calculated the intrinsic Dirac plasmon lifetime as solely due to electron-electron interactions [Eq. (70)] and the background of optical absorption below the single-particle threshold [Eq. (74)].

Suppressed backscattering due to the chiral nature of the eigenstates of the massless Dirac fermion Hamiltonian yields plasmon lifetimes in graphene which are much longer than the corresponding counterparts in ordinary 2D electron gases. Our calculations demonstrate that current samples^{15,16} are not yet in the intrinsic regime. This statement is fully supported by microscopic calculations of the impact of disorder.²⁰ Graphene sheets on h-BN²⁷ or suspended samples²⁸ offer the opportunity to reach the intrinsic regime, where our theoretical predictions can be tested.

ACKNOWLEDGMENTS

We thank A. H. MacDonald and D. M. Basko for useful and stimulating discussions. This work was supported by the BES Grant No. DE-FG02-05ER46203, the EC under Graphene Flagship (Contract No. CNECT-ICT-604391), and

the Italian Ministry of Education, University, and Research (MIUR) through the program ‘‘FIRB - Futuro in Ricerca 2010’’ - Project PLASMOGRAPH (Grant No. RBFR10M5BT).

APPENDIX A: THE INTRINSIC LIFETIME OF A PLASMON IN AN ORDINARY PARABOLIC-BAND 2D ELECTRON GAS

To benchmark our method, in this Appendix we extend the calculations reported in Secs. IV–VI of the main text to the case of a conventional parabolic-band 2DEG.

The 2DEG Hamiltonian (per spin channel) is²

$$\hat{H} = \sum_k \varepsilon_k \hat{c}_k^\dagger \hat{c}_k + \frac{1}{2} \sum_{q'} v_{q'} \sum_{k,k'} \hat{c}_{k-}^\dagger \hat{c}_{k'+}^\dagger \hat{c}_{k'-} \hat{c}_{k+} \equiv \hat{H}_0 + \hat{H}_{ee}. \quad (A1)$$

Here $\mathbf{k}_\pm = \mathbf{k} \pm \mathbf{q}'/2$, $\varepsilon_k = k^2/(2m)$, and $v_q = 2\pi e^2/(\epsilon q)$. Following the procedure outlined in Sec. IV, we determine the generator of the canonical transformation (17) up to first-order in the strength of e-e interactions. Defining

$$i\hat{F}_1 \equiv \frac{1}{2} \sum_{q'} v_{q'} \sum_{k,k'} \mathcal{M}(\mathbf{k}, \mathbf{k}', \mathbf{q}') \hat{c}_{k-}^\dagger \hat{c}_{k'+}^\dagger \hat{c}_{k'-} \hat{c}_{k+}, \quad (A2)$$

and solving $[i\hat{F}_1, \hat{H}_0] = -\hat{H}_{ee}$ [see Eq. (19)] we find

$$\mathcal{M}(\mathbf{k}, \mathbf{k}', \mathbf{q}') = \frac{1}{\varepsilon_{k_-} + \varepsilon_{k'_+} - \varepsilon_{k_+} - \varepsilon_{k'_-}}, \quad (A3)$$

which should be compared with Eq. (32) in the main text.

Following the steps described in the main text, we arrive at the following result for the first-order correction $\hat{j}_{1,q}$ to the transformed current operator \hat{j}'_q :

$$\hat{\mathbf{q}} \cdot \hat{j}_{1,q} = \sum_{q'} v_{q'} \hat{\Upsilon}_{q,q'} \hat{n}_{-q'}, \quad (A4)$$

with

$$\begin{aligned} \hat{\Upsilon}_{q,q'} &= \frac{v_F q_x}{\omega^2} \sum_{\alpha=x,y} \left(\frac{q_y^2}{q'^2} \frac{q'_\alpha}{k_F} - 2 \frac{q'_x}{k_F} \delta_{\alpha,x} \right) \hat{j}_{q',\alpha} \\ &\equiv \sum_{\alpha=x,y} \Gamma_\alpha(\mathbf{q}, \mathbf{q}') \hat{j}_{q',\alpha}. \end{aligned} \quad (A5)$$

Equation (A5) should be carefully compared with Eq. (59). The main differences are: (i) the absence of a chirality factor of the form $1 - q'^2/(4k_F^2)$ in Eq. (A5), and (ii) no term in Eq. (A5) that remains finite in the long-wavelength $\mathbf{q} \rightarrow \mathbf{0}$ limit.

Following the steps outlined in the main text, we obtain that the noninteracting spectrum of $\hat{\mathbf{q}} \cdot \hat{j}_{1,q}$ can be calculated from the four-vertex Feynman diagrams in Figs. 2(a)–2(d), of which the disconnected ones dominate in the large- N_f limit. The final formula for the density-density response function to second order in e-e interactions and in the large- N_f limit is identical to Eq. (60) with $\Gamma_\alpha(\mathbf{q}, \mathbf{q}')$ defined in Eq. (A5). For future purposes we define

$$\begin{aligned} M_{\alpha\beta}(\varphi_{q'}) &\equiv \frac{m^2 \omega^4}{q^2 q'^2} \Gamma_\alpha(\mathbf{q}, \mathbf{q}') \Gamma_\beta(-\mathbf{q}, -\mathbf{q}') \\ &= \{[\cos^2(\varphi_{q'}) + 1] \cos(\varphi_{q'}), -\sin^3(\varphi_{q'})\}_\alpha \\ &\quad \times \{[\cos^2(\varphi_{q'}) + 1] \cos(\varphi_{q'}), -\sin^3(\varphi_{q'})\}_\beta. \end{aligned} \quad (A6)$$

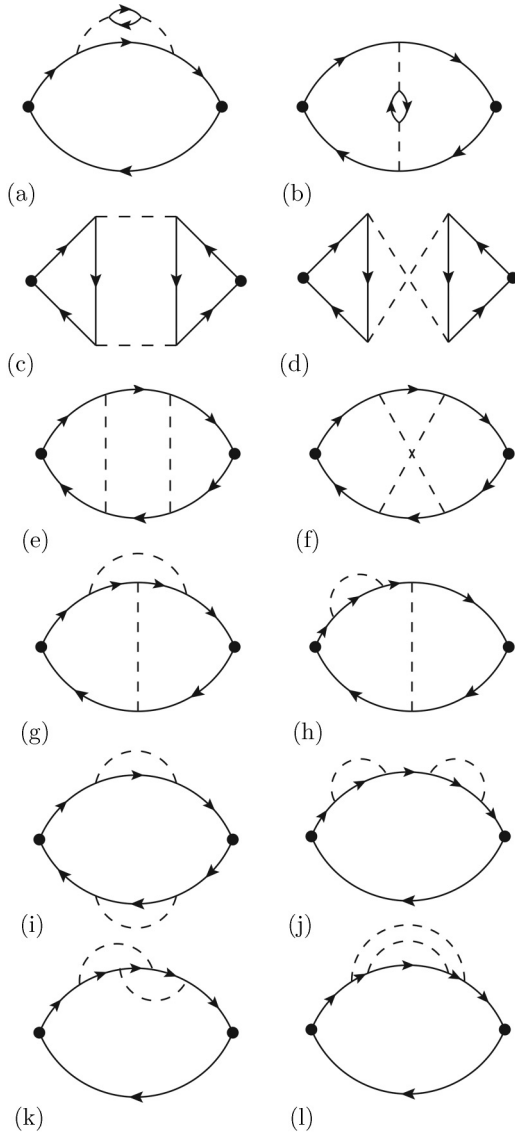


FIG. 8. Second-order (in the strength of e-e interactions) diagrams for the proper longitudinal current-current response function. (a)–(d) are dominant in the large- N_f limit. (a) A diagram with a self-energy insertion, while (b) illustrates a diagram with a vertex correction. Finally, (c) and (d) depict two Aslamazov-Larkin-type diagrams. Solid (dashed) lines represent noninteracting Green's functions (e-e interactions), while filled dots represent current operators at external vertices.

Corresponding numerical results for the intrinsic damping rate of plasmons in a 2DEG are reported in Figs. 3 and 4.

APPENDIX B: THE INTRINSIC LIFETIME OF A PLASMON FROM “BRUTE-FORCE” MANY-BODY DIAGRAMATIC PERTURBATION THEORY

In this Appendix we prove, for the simpler case of the 2DEG, that Eq. (60) with $\Gamma_\alpha(\mathbf{q}, \mathbf{q}')$ as defined in Eq. (A5) is equivalent to a “brute-force” many-body diagrammatic perturbation theory calculation.

In Fig. 8 we show all the second-order Feynman diagrams for the proper² longitudinal current-current response function.

Solid lines are bare propagators while dashed lines represent e-e interactions. Filled circles at external vertices represent 2DEG current operators. To make contact with the main text and in the spirit of a large- N_f expansion, we select only the diagrams that contain the largest number of fermions loops. In what follows we therefore consider only the diagrams in Figs. 8(a)–8(d), which contain *two* fermion loops. As in the main text, we consider the limit of zero temperature.

We start from the diagram in Fig. 8(a), which contains a second-order self-energy insertion on the upper Green's function. After summing it to its time-reversal partner (which contains the second-order self-energy insertion on the lower Green's function) we find

$$\begin{aligned} \chi_{j_x j_x}^{(\text{SE})}(\mathbf{q}, i\omega) = & - \int \frac{d^2 \mathbf{k}}{(2\pi)^2} \int \frac{d^2 \mathbf{k}'}{(2\pi)^2} \int_{-\infty}^{+\infty} \frac{d\varepsilon}{2\pi} \int_{-\infty}^{+\infty} \frac{d\varepsilon'}{2\pi} \\ & \times \frac{k_x^2}{m^2} W(|\mathbf{k} - \mathbf{k}'|, i\varepsilon - i\varepsilon') G^{(0)}(\mathbf{k}_-, i\varepsilon_-) \\ & \times G^{(0)}(\mathbf{k}_+, i\varepsilon_+) [G^{(0)}(\mathbf{k}'_+, i\varepsilon'_+) G^{(0)}(\mathbf{k}_+, i\varepsilon_+) \\ & + G^{(0)}(\mathbf{k}_-, i\varepsilon_-) G^{(0)}(\mathbf{k}'_-, i\varepsilon'_-)]. \end{aligned} \quad (\text{B1})$$

We have introduced the bare (noninteracting) Green's function,

$$G^{(0)}(\mathbf{k}, i\varepsilon_n) = \frac{1}{i\varepsilon_n - \xi_{\mathbf{k}}}, \quad (\text{B2})$$

where $\xi_{\mathbf{k}} = \varepsilon_{\mathbf{k}} - \varepsilon_F$ is the 2DEG band energy $\varepsilon_{\mathbf{k}} = k^2/(2m)$ measured from the Fermi energy ε_F . Moreover,

$$W(\mathbf{Q}, i\Omega) = -v_Q^2 \int_{-\infty}^{+\infty} \frac{d\omega'}{\pi} \frac{\text{Im} \chi_{mn}^{(0)}(\mathbf{Q}, \omega')}{i\Omega - \omega'} \quad (\text{B3})$$

is the spectral representation (see Appendix 14 in Ref. 2) of two interaction lines with a fermion loop (bare bubble or Lindhard function) in between.

The diagram in Fig. 8(b), which contains a vertex correction, reads

$$\begin{aligned} \chi_{j_x j_x}^{(\text{VC})}(\mathbf{q}, i\omega) = & - \int \frac{d^2 \mathbf{k}}{(2\pi)^2} \int \frac{d^2 \mathbf{k}'}{(2\pi)^2} \int_{-\infty}^{+\infty} \frac{d\varepsilon}{2\pi} \int_{-\infty}^{+\infty} \frac{d\varepsilon'}{2\pi} \\ & \times \frac{k_x k'_x}{m^2} W(|\mathbf{k} - \mathbf{k}'|, i\varepsilon - i\varepsilon') G^{(0)}(\mathbf{k}_-, i\varepsilon_-) \\ & \times G^{(0)}(\mathbf{k}_+, i\varepsilon_+) G^{(0)}(\mathbf{k}'_+, i\varepsilon'_+) G^{(0)}(\mathbf{k}'_-, i\varepsilon'_-). \end{aligned} \quad (\text{B4})$$

Finally, the sum of the two Aslamazov-Larkin diagrams in Figs. 8(c) and 8(d) gives

$$\begin{aligned} \chi_{j_x j_x}^{(\text{AL})}(\mathbf{q}, i\omega) = & \frac{1}{4} \int \frac{d^2 \mathbf{q}'}{(2\pi)^2} \int \frac{d\omega'}{\pi} v_{\mathbf{q}' - \mathbf{q}/2} v_{\mathbf{q}' + \mathbf{q}/2} \\ & \times \Gamma(\mathbf{q}' - \mathbf{q}/2, \mathbf{q}' + \mathbf{q}/2, i\omega', i\omega + i\omega') \\ & \times \Gamma(\mathbf{q}' + \mathbf{q}/2, \mathbf{q}' - \mathbf{q}/2, i\omega + i\omega', i\omega'), \end{aligned} \quad (\text{B5})$$

where

$$\begin{aligned} & \Gamma(\mathbf{q}_1, \mathbf{q}_2, i\omega_1, i\omega_2) \\ & \equiv \frac{1}{m} \int \frac{d^2 \mathbf{k}}{(2\pi)^2} \int_{-\infty}^{+\infty} \frac{d\varepsilon}{2\pi} \left(k_x + \frac{q_{1,x} + q_{2,x}}{2} \right) G^{(0)}(\mathbf{k}, i\varepsilon) \\ & \times [G^{(0)}(\mathbf{k} + \mathbf{q}_1, i\varepsilon + i\omega_1) G^{(0)}(\mathbf{k} + \mathbf{q}_2, i\varepsilon + i\omega_2) \\ & - G^{(0)}(\mathbf{k} + \mathbf{q}_2, i\varepsilon - i\omega_2) G^{(0)}(\mathbf{k} + \mathbf{q}_1, i\varepsilon - i\omega_1)]. \end{aligned} \quad (\text{B6})$$

As we will see below, it is mandatory to retain *all* the contributions listed above to find the correct second-order large- N_f result, since important cancellations occur between seemingly different diagrams, in particular those leading to $\text{Re}[\sigma_0(\omega)] = 0$.

1. Calculation of self-energy and vertex corrections

We now briefly describe the procedure we have followed to calculate Eqs. (B1) and (B4).

The easiest way to proceed is to compute the integrals over ε and ε' by utilizing standard methods of complex analysis. These integrals can be calculated by closing the integration contours on the opposite halves of the complex plane, thus

avoiding the poles of $W(\mathbf{Q}, i\Omega)$. The analytical continuation $i\omega \rightarrow \omega + i0^+$ must be carried out only *after* performing the two integrals over ε and ε' .

Importantly, we note that some of the terms in the integrand of $\text{Im}\chi_{j_x j_x}^{(\text{SE})}(\mathbf{q}, \omega)$ and $\text{Im}\chi_{j_x j_x}^{(\text{VC})}(\mathbf{q}, \omega)$ are of the form

$$[\Theta(-\xi_{k_-}) - \Theta(-\xi_{k_+})]\delta(\omega + \xi_{k_-} - \xi_{k_+}), \quad (\text{B7})$$

and therefore vanish when q and ω are outside the particle-hole continuum. Equation (B7) defines indeed the phase space of single electron-hole pair excitations. We recall that we are interested in the regime in which these are absent.

We find that the sum $\text{Im}[\chi_{j_x j_x}^{(\text{SE})}(\mathbf{q}, \omega)] + \text{Im}[\chi_{j_x j_x}^{(\text{VC})}(\mathbf{q}, \omega)]$ reduces, in the long-wavelength $q \rightarrow \mathbf{0}$ limit, to

$$\begin{aligned} \text{Im}\chi_{j_x j_x}^{(\text{VC-SE})}(\mathbf{q}, \omega) = & - \int \frac{d^2 \mathbf{q}'}{(2\pi)^2} \frac{v_{\mathbf{q}'}^2}{m^2} \int_0^\omega \frac{d\omega'}{\pi} \text{Im}\chi_{nn}^{(0)}(\mathbf{q}', \omega') \left[\frac{q_x^2}{\omega^2} \text{Im}\chi_{nn}^{(0)}(|\mathbf{q} + \mathbf{q}'|, \omega - \omega') + q \frac{4q_x^2}{\omega^3} \text{Im}\chi_{n j_x}^{(0)}(\mathbf{q} + \mathbf{q}', \omega - \omega') \right. \\ & \left. + q^2 \frac{10q_x^2}{\omega^4} \text{Im}\chi_{j_x j_x}^{(0)}(\mathbf{q}', \omega - \omega') + q^2 \frac{q_x^4}{2m^2 \omega^4} \text{Im}\chi_{nn}^{(0)}(\mathbf{q}', \omega - \omega') \right]. \end{aligned} \quad (\text{B8})$$

2. Calculation of Aslamazov-Larkin diagrams

We now briefly discuss the steps which are needed to calculate Eq. (B5). More details on the calculation of topologically identical diagrams can be found in Ref. 30.

Integrating Eq. (B6) over the energy ε it is possible to show that the function $\Gamma(\mathbf{q}', \mathbf{q} + \mathbf{q}', i\omega', i\omega + i\omega')$ has two branch cuts for purely imaginary ω' and $\omega + \omega'$. Equation (B5) can thus be calculated by closing the contour in the upper half of the complex ω' plane and excluding the branch cuts. Performing the analytical continuation $i\omega \rightarrow \omega + i0^+$ *after* the contour integration we obtain

$$\begin{aligned} \chi_{j_x j_x}^{(\text{AL})}(\mathbf{q}, \omega) = & i \int \frac{d^2 \mathbf{q}'}{(2\pi)^2} \frac{v_{\mathbf{q}'-q/2} v_{\mathbf{q}'+q/2}}{4m^2} \int_0^\infty \frac{d\omega'}{\pi} [\Gamma_{-+}^{(1)}(-\omega', \omega - \omega') \Gamma_{+-}^{(2)}(\omega - \omega', -\omega') - \Gamma_{++}^{(1)}(-\omega', \omega - \omega') \Gamma_{++}^{(2)}(\omega - \omega', -\omega') \\ & + \Gamma_{--}^{(1)}(-\omega - \omega', -\omega') \Gamma_{--}^{(2)}(-\omega', -\omega - \omega') - \Gamma_{-+}^{(1)}(-\omega - \omega', -\omega') \Gamma_{+-}^{(2)}(-\omega', -\omega - \omega')], \end{aligned} \quad (\text{B9})$$

where we have introduced the shorthands

$$\Gamma_{\lambda_1 \lambda_2}^{(1)}(\omega_1, \omega_2) = \Gamma(\mathbf{q}' - \mathbf{q}/2, \mathbf{q}' + \mathbf{q}/2, \omega_1 + i\lambda_1 \eta, \omega_2 + i\lambda_2 \eta) \quad (\text{B10})$$

and

$$\Gamma_{\lambda_1 \lambda_2}^{(2)}(\omega_1, \omega_2) = \Gamma(\mathbf{q}' + \mathbf{q}/2, \mathbf{q}' - \mathbf{q}/2, \omega_1 + i\lambda_1 \eta, \omega_2 + i\lambda_2 \eta). \quad (\text{B11})$$

It is evident that the imaginary part of $\chi_{j_x j_x}^{(\text{AL})}(\mathbf{q}, \omega)$ coincides with the real part of the integrand on the right-hand side of Eq. (B9). Since $\text{Re}(zw) = \text{Re}(z)\text{Re}(w) - \text{Im}(z)\text{Im}(w)$, the terms contributing to $\text{Im}[\chi_{j_x j_x}^{(\text{AL})}(\mathbf{q}, \omega)]$ can be classified into two groups. One group contains terms proportional to the product $\text{Re}[\Gamma_{\lambda_1 \lambda_2}^{(1)}(\omega_1, \omega_2)]\text{Re}[\Gamma_{\lambda_1 \lambda_2}^{(2)}(\omega_1, \omega_2)]$, while the other contains terms of the form $\text{Im}[\Gamma_{\lambda_1 \lambda_2}^{(1)}(\omega_1, \omega_2)]\text{Im}[\Gamma_{\lambda_1 \lambda_2}^{(2)}(\omega_1, \omega_2)]$. It can be shown that the former group gives a subleading contribution with respect to the latter, in the long-wavelength limit. In this limit we can therefore consider only the terms which contain the product of imaginary parts of the functions $\Gamma_{\lambda_1 \lambda_2}^{(1)}(\omega_1, \omega_2)$ and $\Gamma_{\lambda_1 \lambda_2}^{(2)}(\omega_1, \omega_2)$. Integrating Eqs. (B10) and (B11) over the energy, performing the analytical continuation, and taking the imaginary part, it is easy to show that $\text{Im}\Gamma_{\lambda_1 \lambda_2}^{(1)}(\mathbf{q}_1, \mathbf{q}_2, i\omega_1, i\omega_2) = \text{Im}\Gamma_{\lambda_2 \lambda_1}^{(2)}(\mathbf{q}_2, \mathbf{q}_1, i\omega_2, i\omega_1)$ when q and ω are outside the particle-hole continuum.

After some lengthy but straightforward algebra we get, in the long-wavelength $q \rightarrow \mathbf{0}$ limit,

$$\begin{aligned} \text{Im}\chi_{j_x j_x}^{(\text{AL})}(\mathbf{q}, \omega) = & \int \frac{d^2 \mathbf{q}'}{(2\pi)^2} \frac{v_{\mathbf{q}'} v_{\mathbf{q}'+q}}{m^2} \int_0^\omega \frac{d\omega'}{\pi} \left\{ \frac{q_x^2}{\omega^2} \text{Im}\chi_{nn}^{(0)}(\mathbf{q}', \omega') \text{Im}\chi_{nn}^{(0)}(|\mathbf{q} + \mathbf{q}'|, \omega - \omega') \right. \\ & - q \frac{2q_x^2}{\omega^3} [\text{Im}\chi_{n j_x}^{(0)}(\mathbf{q}', \omega') \text{Im}\chi_{nn}^{(0)}(|\mathbf{q} + \mathbf{q}'|, \omega - \omega') - \text{Im}\chi_{nn}^{(0)}(\mathbf{q}', \omega') \text{Im}\chi_{n j_x}^{(0)}(\mathbf{q} + \mathbf{q}', \omega - \omega')] \\ & \left. + q \frac{q_x^2}{\omega^2} \text{Im}\chi_{nn}^{(0)}(\mathbf{q}', \omega') \text{Im}\chi_{nn}^{(0)}(|\mathbf{q} + \mathbf{q}'|, \omega - \omega') + q^2 \frac{q_x^4}{2m^2 \omega^4} \text{Im}\chi_{nn}^{(0)}(\mathbf{q}', \omega') \text{Im}\chi_{nn}^{(0)}(\mathbf{q}', \omega - \omega') \right\} \end{aligned}$$

$$\begin{aligned}
 & + q^2 \frac{2q'_x}{\omega^3} \left[\text{Im}\chi_{nn}^{(0)}(q', \omega') \text{Im}\chi_{nj_x}^{(0)}(q', \omega - \omega') - \text{Im}\chi_{nj_x}^{(0)}(q', \omega') \text{Im}\chi_{nn}^{(0)}(q', \omega - \omega') \right] \\
 & + q^2 \frac{3q'_x{}^2}{\omega^4} \left[\text{Im}\chi_{nn}^{(0)}(q', \omega') \text{Im}\chi_{j_x j_x}^{(0)}(q', \omega - \omega') + \text{Im}\chi_{j_x j_x}^{(0)}(q', \omega') \text{Im}\chi_{nn}^{(0)}(q', \omega - \omega') \right] \\
 & - q^2 \frac{4q'_x{}^2}{\omega^4} \text{Im}\chi_{nj_x}^{(0)}(q', \omega') \text{Im}\chi_{j_x n}^{(0)}(q', \omega - \omega') \left. \right\}. \quad (\text{B12})
 \end{aligned}$$

3. The small- q expansion

Summing Eqs. (B8) and (B12) it is easy to prove that the coefficients of the terms $O(q^0)$ and $O(q)$ are exactly zero. The latter vanishes upon angular integration over φ_q . After lengthy but straightforward algebraic manipulations it is possible to expand the remainder to $O(q^2)$. The following identities turn out to be useful in the algebraic steps:

$$\begin{aligned}
 & \omega^2 \text{Im}[\chi_{nn}^{(0)}(q', \omega')] \text{Im}[\chi_{nn}^{(0)}(q', \omega - \omega')] \\
 & = 2 \sum_{\alpha, \beta} q'_\alpha q'_\beta \left\{ \text{Im}[\chi_{nn}^{(0)}(q', \omega')] \text{Im}[\chi_{j_\alpha j_\beta}^{(0)}(q', \omega - \omega')] \right. \\
 & \quad \left. + \text{Im}[\chi_{nj_\alpha}^{(0)}(q', \omega')] \text{Im}[\chi_{nj_\beta}^{(0)}(q', \omega - \omega')] \right\} \quad (\text{B13})
 \end{aligned}$$

and

$$\begin{aligned}
 & \omega \text{Im}[\chi_{nn}^{(0)}(q', \omega')] \text{Im}[\chi_{nn}^{(0)}(q', \omega - \omega')] \\
 & = \sum_{\alpha} q'_\alpha \left\{ \text{Im}[\chi_{nn}^{(0)}(q', \omega')] \text{Im}[\chi_{j_x j_\alpha}^{(0)}(q', \omega - \omega')] \right. \\
 & \quad \left. + \text{Im}[\chi_{nj_x}^{(0)}(q', \omega')] \text{Im}[\chi_{nj_\alpha}^{(0)}(q', \omega - \omega')] \right\}, \quad (\text{B14})
 \end{aligned}$$

where $\alpha, \beta = x, y$.

The final expression reads

$$\begin{aligned}
 \text{Im}\chi_{j_x j_x}(q, \omega) & = -\frac{q^2}{m^2 \omega^4} \sum_{\alpha, \beta=x, y} \int \frac{d^2 q'}{(2\pi)^2} \int_0^\omega \frac{d\omega'}{\pi} v_q^2 q'^2 \\
 & \quad \times M_{\alpha\beta}(\varphi_{q'}) \left[\text{Im}\chi_{nn}^{(0)}(q', \omega') \text{Im}\chi_{j_\alpha j_\beta}^{(0)}(q', \omega - \omega') \right. \\
 & \quad \left. + \text{Im}\chi_{nj_\alpha}^{(0)}(q', \omega') \text{Im}\chi_{nj_\beta}^{(0)}(q', \omega - \omega') \right], \quad (\text{B15})
 \end{aligned}$$

where

$$\begin{aligned}
 M_{\alpha\beta}(\varphi_{q'}) & = (\cos(\varphi_{q'})[1 + \cos^2(\varphi_{q'})], -\sin^3(\varphi_{q'})_\alpha \\
 & \quad \times (\cos(\varphi_{q'})[1 + \cos^2(\varphi_{q'})], -\sin^3(\varphi_{q'})_\beta). \quad (\text{B16})
 \end{aligned}$$

Note that the matrix elements in Eq. (B16) coincide with those in Eq. (A6). Equation (B15) can be precisely recast in the form of Eq. (60) with $\Gamma_\alpha(q, q')$ defined in Eq. (A5).

APPENDIX C: THE DEFINITION OF γ_p

The inverse quality factor $\gamma_p(q)$ has been defined in this paper in order to match the definition given in Ref. 15.

The authors of Ref. 15 define the plasmon frequency (which coincides with the external photon frequency ω_{ph}) as a purely real quantity. They introduce a complex plasmon momentum $q_p = q_1 + iq_2$ and define the inverse quality factor $\tilde{\gamma}_p$ as¹⁵

$$\tilde{\gamma}_p \equiv \frac{q_2}{q_1}. \quad (\text{C1})$$

The complex plasmon momentum q_p can be derived by solving the equality

$$\omega_p(q_p) - i\Gamma_p(q_p) = \omega_{\text{ph}}. \quad (\text{C2})$$

Equation (C2) can be solved by expanding it for small q_2 . Neglecting terms of order $q_2\Gamma_p(q_1)$ we find

$$\begin{aligned}
 \omega_p(q_1) & = \omega_{\text{ph}}, \quad (\text{C3}) \\
 q_2 & = \frac{\Gamma_p(q_1)}{\partial\omega_p(q)/\partial q|_{q=q_1}}.
 \end{aligned}$$

As shown after Eq. (10), in the limit $q \rightarrow 0$ the RPA plasmon frequency is given by^{5,12} $\omega_p(q) = \sqrt{2D_0 q/\epsilon}$. This in turn implies that $\partial\omega_p(q)/\partial q = \omega_p(q)/(2q)$, and that

$$\tilde{\gamma}_p = 2 \frac{\Gamma_p(q_1)}{\omega_p(q_1)} = \gamma_p(q_1). \quad (\text{C4})$$

The relation between $\gamma_p(q_1)$ and the ratio $\text{Re}[\sigma(q, \omega)]/\text{Im}[\sigma(q, \omega)]$ for $q = q_1$ and $\omega = \omega_p(q_1)$ can be derived by using the following well-known relation:²

$$\chi_{nn}(q, \omega) = \frac{q^2}{ie^2\omega} \sigma(q, \omega) \quad (\text{C5})$$

in Eq. (10), which immediately gives

$$\Gamma_p(q) = \frac{\text{Re}[\sigma(q, \omega)]}{\frac{\partial\text{Im}[\sigma(q, \omega)]}{\partial\omega} - \frac{\text{Im}[\sigma(q, \omega)]}{\omega}} \Bigg|_{q=q_1, \omega=\omega_p(q_1)}. \quad (\text{C6})$$

Since the imaginary part of the RPA conductivity scales like ω^{-1} in the region of interest, we get $\partial\text{Im}[\sigma(q, \omega)]/\partial\omega = -\text{Im}[\sigma(q, \omega)]/\omega$, which in turn implies

$$\gamma_p(q_1) = \frac{\text{Re}[\sigma(q_1, \omega_p(q_1))]}{\text{Im}[\sigma(q_1, \omega_p(q_1))]} \quad (\text{C7})$$

*principia@missouri.edu

¹D. Pines and P. Nozières, *The Theory of Quantum Liquids* (W. A. Benjamin, New York, 1966).

²G. F. Giuliani and G. Vignale, *Quantum Theory of the Electron Liquid* (Cambridge University Press, Cambridge, 2005).

³S. A. Maier, *Plasmonics—Fundamentals and Applications* (Springer, New York, 2007).

⁴T. W. Ebbesen, C. Genet, and S. I. Bozhevolnyi, *Phys. Today* **61**, 44 (2008); L. Novotny, *ibid.* **64**, 47 (2011); M. I. Stockman, *ibid.* **64**, 39 (2011).

- ⁵K. W.-K. Shung, *Phys. Rev. B* **34**, 979 (1986); B. Wunsch, T. Stauber, F. Sols, and F. Guinea, *New J. Phys.* **8**, 318 (2006); E. H. Hwang and S. Das Sarma, *Phys. Rev. B* **75**, 205418 (2007); M. Polini, R. Asgari, G. Borghi, Y. Barlas, T. Pereg-Barnea, and A. H. MacDonald, *ibid.* **77**, 081411(R) (2008); A. Principi, M. Polini, and G. Vignale, *ibid.* **80**, 075418 (2009); M. Jablan, H. Buljan, and M. Soljačić, *ibid.* **80**, 245435 (2009).
- ⁶S. H. Abedinpour, G. Vignale, A. Principi, M. Polini, W.-K. Tse, and A. H. MacDonald, *Phys. Rev. B* **84**, 045429 (2011).
- ⁷M. Orlita, I. Crassee, C. Faugeras, A. B. Kuzmenko, F. Fromm, M. Ostler, T. Seyller, G. Martinez, M. Polini, and M. Potemski, *New J. Phys.* **14**, 095008 (2012).
- ⁸L. S. Levitov, A. V. Shtyk, and M. V. Feigelman, arXiv:1302.5036.
- ⁹K. S. Novoselov and A. K. Geim, *Nat. Mater.* **6**, 183 (2007).
- ¹⁰A. H. Castro Neto, F. Guinea, N. M. R. Peres, K. S. Novoselov, and A. K. Geim, *Rev. Mod. Phys.* **81**, 109 (2009).
- ¹¹V. N. Kotov, B. Uchoa, V. M. Pereira, F. Guinea, and A. H. Castro Neto, *Rev. Mod. Phys.* **84**, 1067 (2012).
- ¹²A. N. Grigorenko, M. Polini, and K. S. Novoselov, *Nat. Photon.* **6**, 749 (2012).
- ¹³L. Ju, B. Geng, J. Horng, C. Girit, M. Martin, Z. Hao, H. A. Bechtel, X. Liang, A. Zettl, Y. Ron Shen, and F. Wang, *Nat. Nanotech.* **6**, 630 (2011).
- ¹⁴Z. Fei, G. O. Andreev, W. Bao, L. M. Zhang, A. S. McLeod, C. Wang, M. K. Stewart, Z. Zhao, G. Dominguez, M. Thiemens, M. M. Fogler, M. J. Tauber, A. H. Castro-Neto, C. N. Lau, F. Keilmann, and D. N. Basov, *Nano Lett.* **11**, 4701 (2011).
- ¹⁵Z. Fei, A. S. Rodin, G. O. Andreev, W. Bao, A. S. McLeod, M. Wagner, L. M. Zhang, Z. Zhao, M. Thiemens, G. Dominguez, M. M. Fogler, A. H. Castro Neto, C. N. Lau, F. Keilmann, and D. N. Basov, *Nature (London)* **487**, 82 (2012).
- ¹⁶J. Chen, M. Badioli, P. Alonso-González, S. Thongrattanasiri, F. Huth, J. Osmond, M. Spasenović, A. Centeno, A. Pesquera, P. Godignon, A. Zurutuza Elorza, N. Camara, F. J. García de Abajo, R. Hillenbrand, and F. H. L. Koppens, *Nature (London)* **487**, 77 (2012).
- ¹⁷H. Yan, X. Li, B. Chandra, G. Tulevski, Y. Wu, M. Freitag, W. Zhu, P. Avouris, and F. Xia, *Nat. Nanotech.* **7**, 330 (2012).
- ¹⁸L. Vicarelli, M. S. Vitiello, D. Coquillat, A. Lombardo, A. C. Ferrari, W. Knap, M. Polini, V. Pellegrini, and A. Tredicucci, *Nat. Mater.* **11**, 865 (2012).
- ¹⁹H. Yan, T. Low, W. Zhu, Y. Wu, M. Freitag, X. Li, F. Guinea, P. Avouris, and F. Xia, *Nat. Photon.* **7**, 394 (2013).
- ²⁰A. Principi, G. Vignale, M. Carrega, and M. Polini, *Phys. Rev. B* **88**, 121405(R) (2013).
- ²¹We discuss electron doping for the sake of definiteness: τ_p is a particle-hole symmetric quantity.
- ²²M. Hasegawa and M. Watabe, *J. Phys. Soc. Jpn.* **27**, 1393 (1969); A. J. Glick and W. F. Long, *Phys. Rev. B* **4**, 3455 (1971); M. E. Bachlechner, W. Macke, H. M. Miesenböck, and A. Schinner, *Physica B* **168**, 104 (1991); M. E. Bachlechner, H. M. Böhm, and A. Schinner, *Phys. Lett. A* **178**, 186 (1993); H. M. Böhm, S. Conti, and M. P. Tosi, *J. Phys.: Condens. Matter* **8**, 781 (1996).
- ²³R. Nifosi, S. Conti, and M. P. Tosi, *Phys. Rev. B* **58**, 12758 (1998).
- ²⁴For graphene $N_f = 4$ from spin and valley degrees of freedom.⁹⁻¹²
- ²⁵J. Sabio, J. Nilsson, and A. H. Castro Neto, *Phys. Rev. B* **78**, 075410 (2008).
- ²⁶Strictly speaking, in what follows we compute the *proper* current-current response function [usually denoted as $\tilde{\chi}_{AB}(\omega)$], which is defined as the sum of all the diagrams that cannot be divided into two parts by cutting a single interaction line.² Note that the proper response function $\tilde{\chi}_{AB}(\omega)$ coincides with $\chi_{AB}(\omega)$ in the $q \rightarrow 0$ limit.
- ²⁷C. R. Dean, A. F. Young, I. Meric, C. Lee, L. Wang, S. Sorgenfrei, K. Watanabe, T. Taniguchi, P. Kim, K. L. Shepard, and J. Hone, *Nat. Nanotech.* **5**, 722 (2010).
- ²⁸K. I. Bolotin, K. J. Sikes, Z. Jiang, M. Klima, G. Fudenberg, J. Hone, P. Kim, and H. L. Stormer, *Solid State Commun.* **146**, 351 (2008).
- ²⁹M. R. Ramezani, M. M. Vazifeh, R. Asgari, M. Polini, and A. H. MacDonald, *J. Phys. A* **42**, 214015 (2009).
- ³⁰M. Carrega, T. Tudorovskiy, A. Principi, M. I. Katsnelson, and M. Polini, *New J. Phys.* **14**, 063033 (2012).